1-1-1975

A study of gold thin films as formed by pulsed current electrodeposition.

David L. Rehrig

A STUDY OF GOLD THIN FILMS AS FORMED BY PULSED CURRENT ELECTRODEPOSITION

by

David L. Rehrig

A Thesis

Presented to the Graduate Committee

of Lehigh University

in Candidacy for the Degree of

Master of Science

in Metallurgy and Materials Science

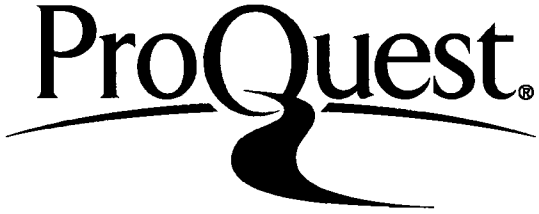

CERTIFICATE OF APPROVAL

This thesis is accepted and approved in partial fulfillment of the requirements for the degree of Master of Science.

April 6, 1975
Date

Co-Professor in Charge

Co-Professor in Charge

Chairman of the Department of Metallurgy and Materials Science

Acknowledgments

The author expresses his appreciation to R. B. Snyder, Western Electric-Allentown for sponsoring this investigation. He also appreciates the help and suggestions of many of the electroplaters at Western Electric, Allentown. Special thanks is extended to R. A. Mantz for his aid with the x-ray aspects of the study and B. M. Keller for her assistance with sample preparation. Acknowledgment is also extended to R. Haynes of Western Electric, Princeton for his interest and discussion concerning pulse electroplating.

Table of Contents

Table of Contents (Cont'd)

Table of Contents (Cont'd)

List of Tables

List of Figures

List of Figures (Cont'd)

List of Figures (Cont'd)

Abstract

An investigation was made into the characteristics of gold deposits as formed by pulsed current. The aspects examined were 1.) porosity 2.) thickness distribution 3.) microstructure 4.) preferred orientation 5.) internal stress 6.) throwing efficiency 7.) cathode efficiency and 8.) pulse waveform.

It was determined by the electrographic and nitric acid tests that gold deposits formed by pulsed current are less porous than deposits formed by electron gun-evaporation, D.C. plating, and asymmetric A.C. plating. The crystallographic differences in gold films formed by these methods were examined by scanning electron microscopy and related to the porosities of the films.

The duration of the pulse current flow (ON Time) and the duration of relaxation (OFF Time) as well as the duty cycle i.e. the percent ratio of ON to the sum of ON and OFF Time, are controllable in pulse plating. Collectively the pulse variations are referred to as waveforms. The porosities of deposits produced by 30 different pulse waveforms were examined by the electrographic porosity test. Porosity correlated with the thickness distribution at short duty cycles ($< 50\%$) but did not follow a pattern at long duty cycles ($\geq 50\%$). Thickness distribution across planar films formed by pulse deposition were comparable to D. C. plated films.

Examination of the microstructure by scanning electron microscopy indicated a variation in grain structure which followed changes in the pulse waveform. This correlation is partially explainable through consideration of nucleation rate. A study of preferred orientation by x-ray diffraction provided evidence which further elucidates the effect of the pulse waveform on the nature of grain growth. The shifts in orientation from (111) texture to dual (111)-(200) corresponded to changes in nucleation density. Stresses in

pulse-plated films with dual (111)-(200) orientation were compared to D.C. plated films with (111) orientation. The pulse-plated gold exhibited a shift from tensile to compressive stress with increasing thickness, the D.C. plated films were always tensile. Sorption and volume expansion mechanisms were suggested to be operative stress models in the pulsed deposits.

Throwing efficiency and throwing power were measured using the Haring Cell. These values quantify the capability to produce uniform thickness on non-planar substrates. Throwing ability varied with cathode efficiency except with 8 and 9 msec ON times where throwing efficiency increased while cathode efficiency decreased. Cathode efficiency is a measure of the percentage current being employed to deposit the metal. At the long ON times, (8 and 9 msec) the metal ions adjacent to the cathode were depleted and hydrogen evolution occurred. The effect of the rectifier characteristics and the electrochemical system on both waveform and cathode efficiency was significant. Pulse rectifiers must have rapid, voltage-rise times in order to deposit films at a high cathode efficiency. If the voltage pulse is distorted, the interaction of the current with the electrochemical system cannot entirely result in metal deposition. This was the case in gold deposition when pulse current was produced by a rectifier having a sluggish rise in voltage. In summary, both variations and distortions of pulse waveform were observed to affect the properties of gold deposits and the efficiencies of gold deposition.

I. Introduction

A. Foreword

In recent years the rapid growth of thin film technology accelerated by the advent of silicon integrated circuits (SIC's) has placed many demands on gold as an electronic material. During 1975 most of the gold fabricated in the United States will be used in electronic devices. The complimentary nature of chemical inertness with high electrical conductivity has gained gold its prominence as a material in electronic technology.

More economical and selective than sputtering and evaporation, electrodeposition has become the most desirable method for process deposition of gold. Microscopic conductive paths, which weave through hundreds of transistors on SIC's smaller than a needle's eye, are electroplated. Micron thick layers, which protect underlying resistors while carrying electrons in the film circuits, are also electroplated. Gold contacts, leads, and connectors, which intertwine circuits together, are all electroplated. Gold electroplating has gathered attention with increasing gold usage, stimulating curiosity into the nature of electrodeposited gold.

Knowledge of the properties obtainable using fixed deposition parameters is desirable to tailor specific deposits to specific applications. Where large areas are blanket plated, thickness uniformity is the paramount concern, but for deposition on contoured substrates throwing efficiency is most important.

In these applications, as in many others which are industrially significant, one plating system may be unable to provide optimum deposition for all situations. Variations in bath chemistry, when it is a viable approach for changing the properties of a deposit, is costly, time consuming, and often irreversible. In the last decade, power supplies have become commercially available which allow industrial electroplaters to vary the form of the current used in electrodeposition. By changing settings on a rectifier, alteration of deposit properties occur without having to alter the bath's chemical composition.

B. Purpose

The purpose of this thesis is to investigate the properties of gold deposits formed by pulsed current waveforms with the bath chemistry held constant. The historical development of current variations in electroplating is considered. Comparisons between pulse plating and other deposition methods used in electronics manufacturing are made where these could be drawn. Differences in properties resulting from variations in current waveforms are examined and reported. The properties considered are:

1. Porosity
2. Microstructure
3. Preferred Orientation
4. Stress
5. Thickness Distribution
6. Throwing Efficiency
7. Current Efficiency

C. Definitions

Pulse plating is a method of electroplating where current is passed through an electrochemical system at controlled frequencies in discrete square wave pulses.

The pulse waveform is described in terms of: ON time, OFF time, duty cycle, peak current density, average current density, and frequency. The waveform in Figure 1 depicts two complete cycles. The duration of the current flow, without interruption, is the ON time, T_A. Similarly, the duration of the interruption when no current is flowing is the OFF time, T_B. The duty cycle is the relationship between ON time and OFF time. Duty cycle is defined by the ratio of ON time to ON time plus OFF time, the total cycle period.

$$\% \text{ Duty Cycle} = \frac{100\ T_A}{T_A + T_B}$$

The peak current density is the quantity of current flowing during the ON time divided by the area of the sample, A_S, being plated.

FIG. 1 PULSE CURRENT WAVEFORM

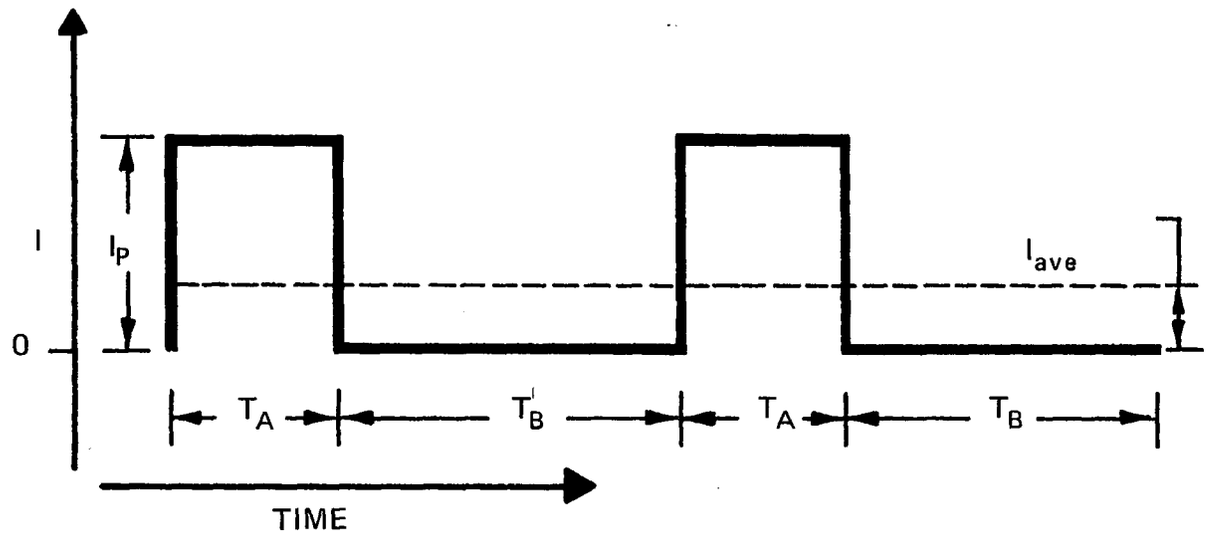

T_A = ON TIME (msec)

T_B = OFF TIME (msec)

$$\% \text{ DUTY CYCLE} = \frac{100\, T_A}{T_A + T_B}$$

I_P = PEAK CURRENT

I_{ave} = AVERAGE CURRENT

$$\text{Peak Current Density} = \frac{I_A}{A_S}$$

The average current density is the mean current flow per area for the total cycle of ON and OFF time:

$$\text{Average Current Density} = \frac{I_A T_A}{A_S (T_A + T_B)}$$

The frequency, ν, is the number of complete cycles per second.

$$\nu = \frac{1 \text{ sec}}{T_A + T_B}$$

D. Historical Background

The electrodeposition of gold by D. C. current was first reported by Brugnatelli in 1805.[1] Since that time advances in gold electroplating have primarily resulted through improvements in bath chemistry. During the last decade, electronic developments have produced refinement and general availability of non-D.C. power supplies. Attention has focused on a largely uninvestigated parameter in electrodeposition, the current waveform.

The observation of non-D.C. current in electrochemical systems dates back to nearly the beginning of gold electroplating. During the 19th century it was found that A.C. and A.C. superimposed on D.C. had a frequency dependent effect on the corrosion rate of metals in electrolysis systems.[2] The decreased polarization and the A.C. frequency dependence of corrosion were well characterized by 1909, when Wohlwill [3] reported the first commercial application of superimposed A.C. on D. C. The Wohlwill method is used to control anodic corrosion in gold refining.

A refinement of A.C. waveforms was the periodic reverse current method first described by Rosing in 1896.[4] Patents were filed during the first half of the twentieth century on various plating methods with periodic reverse current.[5-9]

It was not until 1931 that Winkler[10] introduced pulsed D.C. current to electroplating. Certain nickel-gold alloy compositions that could not be plated by other methods, could be deposited by pulsed current. This phenomenon has since been verified with other alloys such as iron-nickel [11] and silver-tin.[12]

Detailed reviews of the historical evolution in non-D.C. plating are to be found in excellent articles by Baeyens[13] and more recently by Wan, Cheh, and Linford.[14]

E. Reported Advantages

The advantages of pulse over continuous deposition fall into three general areas: alloy plating, deposition rate, and deposit structure.

The application of pulsed current to alloy deposition was noted in the section reviewing the historical development. Alloy deposition is the best established advantage of the technique. Alloys which cannot be deposited by D.C. have been formed by pulsing. In addition the homogeneity of pulse plated alloys is significantly greater than that of similar alloys plated with D.C. current. [11,12]

The reported increase in limiting current density, i.e. maximum deposition rate, is nebulous. Theoreticians debate the nature and extent of the increase. One group[15,16] asserts that the limiting overall plating rate is lower than with direct current. Ozerov et al.[17] report that the plating rate could be increased indefinitely by decreasing the pulse cycle. Avila and Brown[18] report increased deposition rates. These differences appear to result from variations in terms and premises. A discussion of the semantics and assumptions is available.[14] This recent report, confirms and clarifies a slight increase in the practical, though not the theoretical,deposition rates.

The effect of pulsed current on the deposit structure forms a significant portion of the experimental content of this thesis. Earlier studies[19-23] have shown fine grained copper deposits are formed by pulsed deposition. Lamb reports no difference in the structure of copper and silver deposited by pulse compared to D.C. current.[24] Differences in structure

have been reported for tin, chromium,[26] zinc, [23] and nickel.[27] An increase in electrical conductivity over D.C. plated gold has been reported in pulse plated gold films[18] a fact which is indicative of a denser deposit.

II. Porosity

A. Introduction

The integrity of the protection provided by gold films to underlying layers is limited by the porosity of the film. Porosity is the amount of discontinuity in the film which gives exposure to the sub film material. The effect of porosity in manufacturing electrical contacts has been a subject of major investigation.[27] The corrosion of base metals through porous gold in these contacts has been studied,[28] as well as means of inhibiting such corrosion.[29] Corrosion products adversely effect contact resistance, degrading the reliability of the connector. Electrical contacts are generally electroplated hard-gold, usually gold-cobalt alloys, which must withstand mechanical as well as chemical wear.

In thin film circuitry, thin layers of pure gold are deposited on metallized ceramic substrates by either electroplating or evaporation. The gold film acts as both a protective and conductive layer. During circuit fabrication thin film systems are subjected to a variety of hostile process chemicals and ambient vapors, such as hydrofluoric acid, nitric acid, and strong organic acids. If extensive porosity exists, degradation of the device and loss of film adherence can occur. For example, in the case where the underlying film is fabricated as a resistor, rapid aging and high noise levels resulting from changes at the conductor-resistor interface would be anticipated to accompany chemical penetration of the gold film. Potential problems of this type illustrate the cause of concern with porosity in thin, pure gold deposits such as those used in thin film circuitry.

The object of the porosity study was threefold. First, the thickness dependence of porosity for gold thin films deposited by different methods was to be studied. These deposition methods were: (1) D.C. plating, (2) asymmetric A.C. plating, (3) pulse plating, and (4) electron gun evaporation. Second, the microstructure of the films deposited by each method was to be examined. Third, the porosity of pulse plated films deposited by

different waveforms was determined.

B. Experimental Procedure

1. Specimen Preparation

The base substrate for the method-comparison specimens was a high alumina ceramic, measuring 113 mm x 95 mm (4-½" x 3-¾"). The ceramic substrates were examined for surface roughness with a diamond stylus profilometer. The average center line roughness was approximately one micron. This procedure was followed to insure substrates of similar surface finish. Garte[30] has shown porosity is dependent upon substrate roughness, therefore, it was desired to hold this parameter constant.

The ceramic substrate was metallized in an electron gun evaporator with films of titanium, palladium, and copper; 750 angstroms, 3000 angstroms, and 25,000 angstroms thick, respectively. The samples which were to have an evaporated gold film remained, and the gold layer was deposited in situ. The evaporator was a carousel, continuous process, electron gun evaporation system. The gold films were deposited using an electron gun with six kilowatts emission power.

The D.C. plated specimens were plated at an average current density of 2.3 amps. per square foot. Pulse plated specimens were plated at the same current density with a 9% duty cycle i.e. 0.9 msec. ON, 9 msec. OFF. The asymmetric A.C. specimens were plated at a current density of 2.1 amps. per square foot with a three to one ratio in forward to reverse current flow. All plating was in a gold citrate bath containing dibasic ammonium citrate (75 g/l), ammonium sulfate (75 g/l), and potassium gold cyanide (20 g/l). The bath was operated at 65°C and a pH of 5.5 to 6.0. These plating conditions have been found to

provide optimal physical properties for thin film circuit applications.

From each specimen five samples were laser scribed: Two sections 113 mm x 10 mm (4-½" x 3/8") and three sections 113 mm x 25 mm (4-½" x 1"). The smaller samples were used for thickness determinations and the electron microscopy studies. The larger samples were used for the nitric acid and electrographic porosity tests.

Sixty additional samples were pulse plated at the conditions listed in Table 1. Two samples at each duty cycle and ON time – OFF time combination were deposited with a thickness of 8000 Å (0.8 micron). These samples were deposited on Hull Cell brass panels for certainty of reproducible substrate surfaces.

2. Porosity Measurement by Electrographic Tester

Porosity in the gold films was examined by two methods: (1) the electrographic test and (2) the nitric acid test. The electrographic test apparatus was a commercially available instrument manufactured by Meaker Company, a division of Sel Rex, Inc. Indicator paper containing cadmium sulfide (CdS) is placed between an absorbent pad and the sample. Pressure applied by a hydraulic press forces electrolyte into discontinuites in the gold film. Current is applied such that the sample acts as an anode and the press plate as a cathode. The potential across sample and press plate drives migration of Cu++ ions in the electrolyte through the gold to the indicator paper. At the indicator Cu++ ions reacts with CdS to form copper sulfide (CuS), a black compound.

Black dots are apparent on the yellow indicator paper where porosity has allowed passage of Cu++ through the gold film to the indicator paper. The black dot pattern maps pore locations. The tester was operated at 1000 psi, 260 ma current, and 12 volts potential for thirty seconds.

TABLE 1: PULSE WAVEFORMS

NUMBER	DUTY CYCLE (%)	ON TIME (msec)	OFF TIME (msec)	PEAK CURRENT (amp)
1	9	0.1	1.0	7.3
2	9	0.3	3.0	7.3
3	9	0.5	5.0	7.3
4	9	0.7	7.0	7.3
5	9	1.0	10	7.3
6	9	2.0	2.0	7.3
7	9	4.0	40	7.3
8	9	6.0	60	7.3
9	9	8.0	80	7.3
10	9	9.0	90	7.3
11	25	1.0	3.0	2.9
12	33	0.5	1.0	2.2
13	33	1.0	2.0	2.2
14	33	2.0	4.0	2.2
15	33	4.0	8.0	2.2
16	33	6.0	12	2.2
17	33	8.0	16	2.2
18	33	9.0	18	2.2
19	50	1.0	1.0	1.5
20	50	2.0	2.0	1.5
21	50	4.0	4.0	1.5
22	50	6.0	6.0	1.5
23	50	8.0	8.0	1.5
24	50	9.0	9.0	1.5
25	66	2.0	1.0	1.1
26	66	4.0	2.0	1.1
27	66	8.0	4.0	1.1
28	75	6.0	2.0	1.0
29	75	9.0	3.0	1.0
30	90	9.0	1.0	0.8

3. The Nitric Acid Test

To supplement the electrographic test, the nitric acid test for porosity was also performed on each of the gold films. The bottom of a glass desiccator is sealed and the nitric acid vapor allowed to equilibrate in the chamber for thirty minutes. The gold films are then placed in the chamber for one hour, after which they are removed and dried in an oven at 105° C for thirty minutes. The film is then examined for the blue corrosion product, copper nitrate, which forms as crystals which protrude to the gold surface where discontinuity has allowed nitric acid vapor to penetrate the gold film.

The nitric acid test is often used as a manufacturing method for examining porosity. This test is used qualitatively to determine the presence of a porous film. Comparisons with the electrographic records showed reasonable correlation between these tests; no attempt was made to quantify the results of the nitric acid test. It was performed primarily to determine if samples which did not show porosity by the electrographic test would manifest porosity in the nitric acid test. Differences were not detected. The nitric acid test is simple and actually simulates corrosion attack which could occur in manufacturing ambients.

4. Examination of Microstructure

The structure of the films deposited by each plating techniques, D.C., pulse and asymmetric A.C., as well as the films deposited by evaporation was examined by scanning electron microscopy. Photomicrographs of the microstructure were taken using the secondary electron mode of the SEM. The technique provides images with detail, magnification, and depth of field unavailable from optical microscopy.

C. Results

The black dotted patterns for the electrographic test, as well as the blue-green patterns from the nitric acid test, provided an illustrated record of porosity in the samples. In order to quantify these results, dots on the electrographic indicator paper were counted over a unit area. For highly porous samples, four 3.13 cm^2 (0.5 in^2) areas were taken over the sample's pattern and averaged. On slightly porous samples, all dots were counted.

The film thicknesses were recorded to the nearest 0.5 micron with the exception of one 0.2 micron sample. Visual examination of the copper nitrate crystals formed by the nitric acid test qualitatively verified the results of the electrographic test. No attempt was made to quantify the nitric acid test results, nor to make any further comparison between it and the electrographic test. Plots of porosity versus gold film thickness summarize the experimental findings.

Gold films of similar thickness show striking differences in porosity dependent upon deposition technique (Figure 2). The evaporated films were by far the most porous exhibiting 1300 dots/square inch in a sample seven microns thick. At this thickness the plated films did not exhibit any porosity. Thickness greater than seven microns could not be evaporated by the equipment available. Significant porosity was thus present throughout the thickness deposition range of this technique.

At low thickness asymmetric A.C. deposited films manifested less porosity (162 dots/square inch at 1.5 microns) than evaporated (1500 dots/square inch at 2 microns) or D.C. plated (544 dots/square inch at 1.5 microns).

The D.C. plated films exhibited the greatest porosity amongst the plated specimens. High porosity (850 dots/square inch at 0.5 microns) at low thicknesses reduced rapidly as the thickness increased. Pulse plated films exhibited the least porosity of all the deposition techniques, with 125 dots per square inch at 0.5 micron diminishing to no porosity

FIG. 2: RELATIONSHIP BETWEEN POROSITY AND THICKNESS OF GOLD FILMS DEPOSITED BY: ELECTRON GUN EVAPORATION, ASYMMETRIC A.C. PLATING, D.C. PLATING, AND PULSE PLATING.

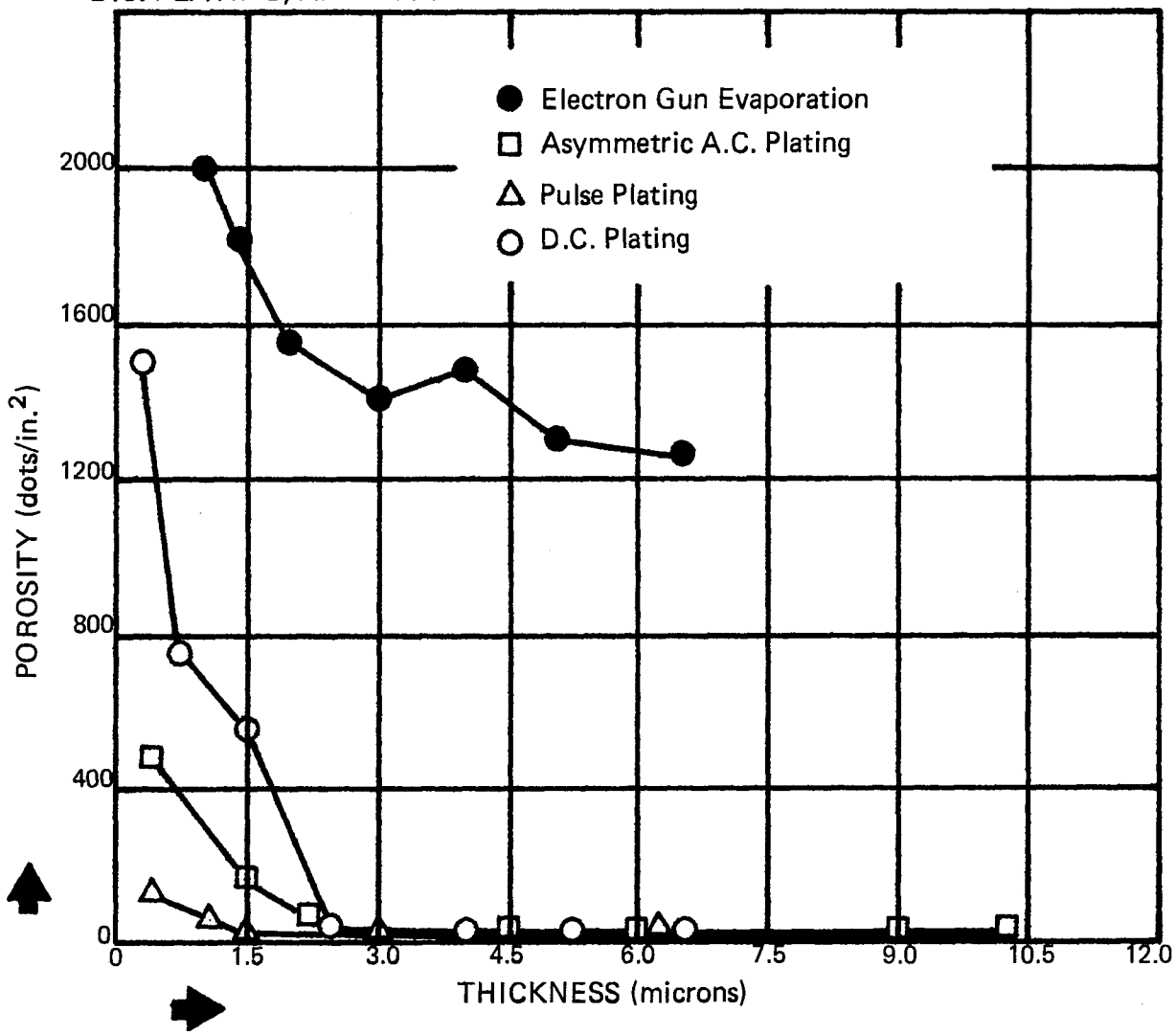

detectable at thicknesses greater than four microns.

The variation of porosity with pulse waveform is shown in Figures 3-6. The porosity and the thickness distribution are plotted on the same log-log coordinates against ON time. The determination of thickness distribution is described in detail in the next section. At the low duty cycles (Figs. 3 and 4) i.e. 9% and 33%, the pattern of the porosity levels follows that of the thickness distribution. The distribution is an indication of the range in thickness of the film which is nominally 0.8 micron based on weight gain. The dependence of porosity on thickness within a single continuous film is evidenced by the parallel pattern of porosity and thickness distribution. As the thickness range above and below the nominal 0.8 micron increases, the porosity increased due to the contribution of pores present in thinner portions of the film. At 9% and 33% duty cycles this pattern is apparent while no effect of ON time on porosity is readily observed.

At longer duty cycles i.e. 50% and greater, the same pattern of parallel thickness distribution and porosity is not observed (Figures 5 and 6). At the 50% duty cycle porosity increased with the duration of the ON time while thickness distribution decreased. At higher duty cycles, $>$ 50%, trends in porosity with neither thickness distribution nor ON time were apparent (Figure 6). The mean porosity value for all pulse plated samples 0.8 micron thick was 93 pores/in^2.

D. Discussion

Porosity has been shown to be dependent on a number of parameters. Garte[30,31] has shown the effects of substrate roughness. Leeds and Clarke[32] have shown the effects of bath composition, electrolyte temperature, pH, and current density on porosity in electroplated films. It is clear that a wide variety of variables can effect the presence of pores in gold films. The origin of pores has not been as extensively studied. Nobel, Ostrow, and Thompson[33] have shown that pores result from surface defects of the

FIG. 3: 9% DUTY CYCLE, LOG POROSITY vs. LOG ON TIME AND LOG THICKNESS DISTRIBUTIONS vs. LOG ON TIME

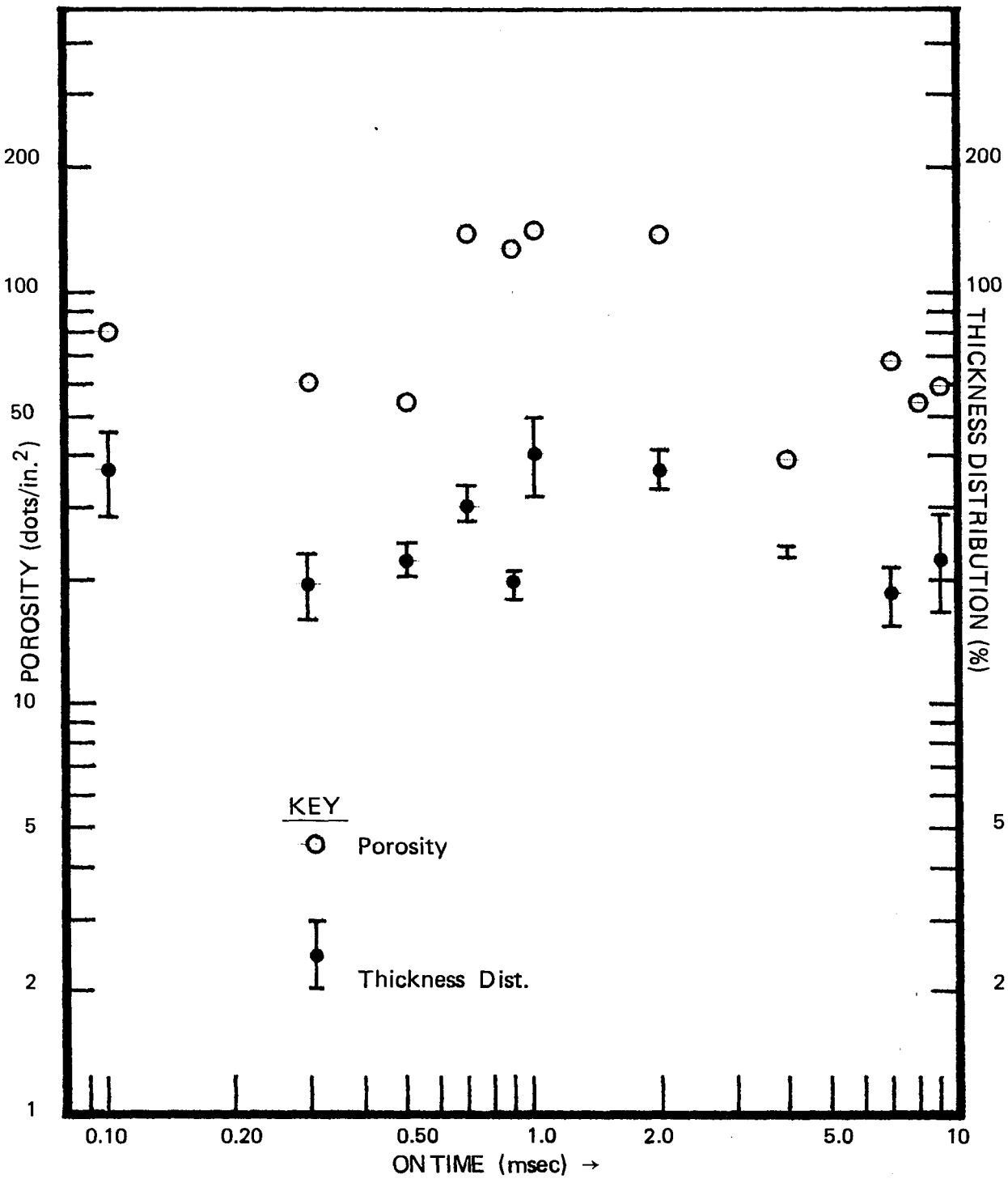

FIG. 4: 33% DUTY CYCLE, LOG POROSITY vs. LOG ON TIME AND LOG THICKNESS DISTRIBUTION vs. LOG ON TIME

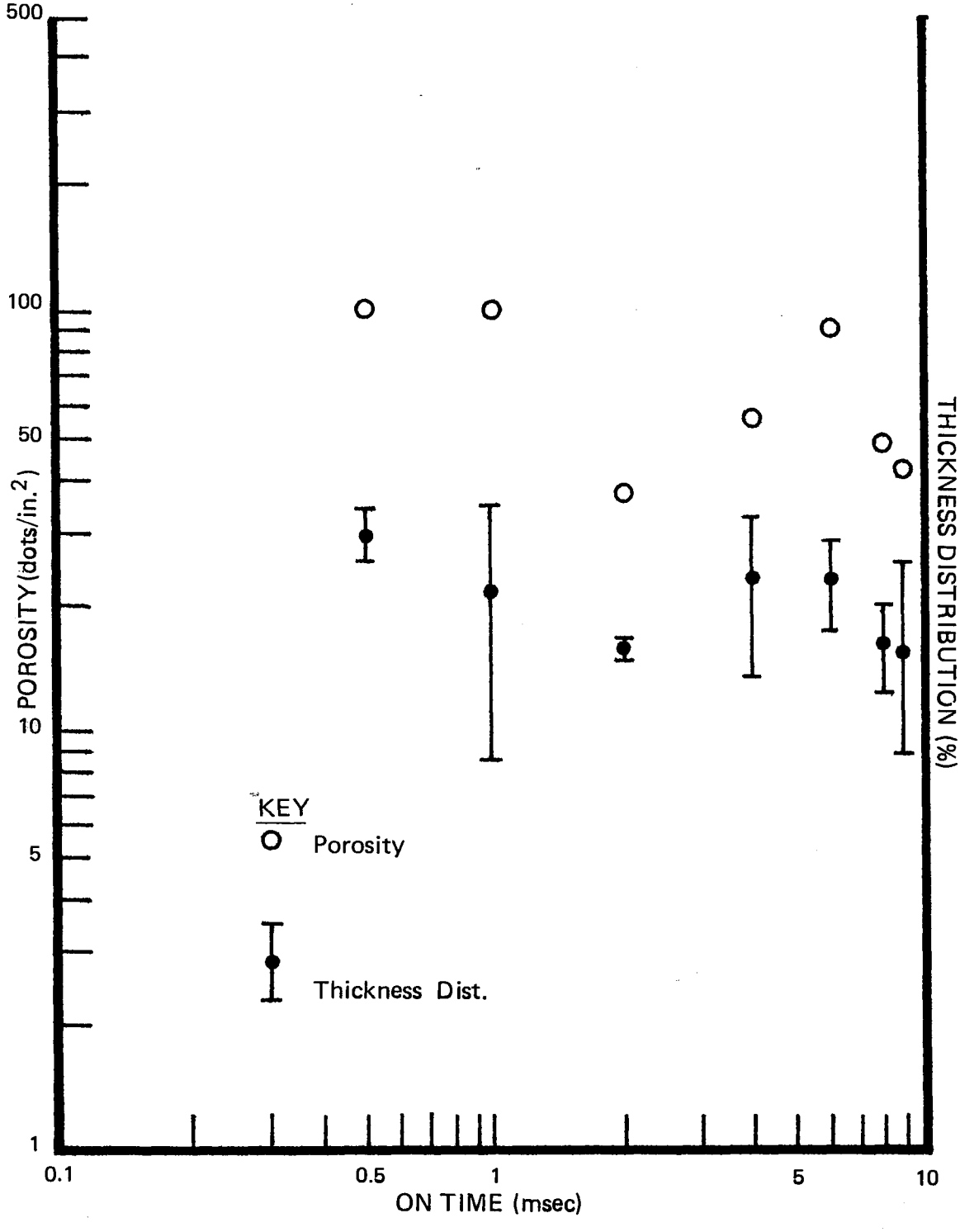

FIG. 5: 50% DUTY CYCLE, LOG POROSITY vs. LOG ON TIME AND LOT THICKNESS DISTRIBUTION vs. LOG ON TIME

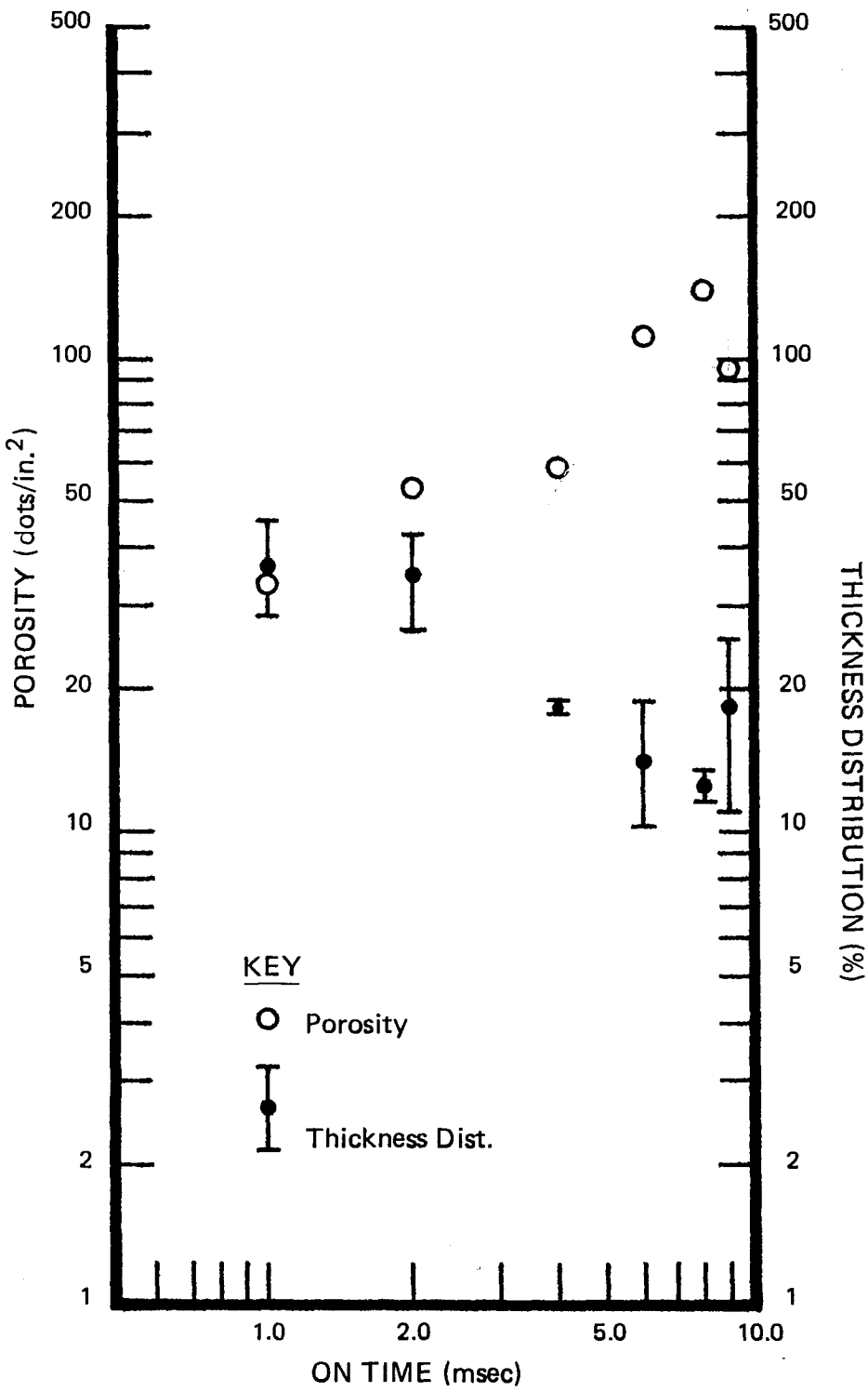

FIG. 6: LOG POROSITY vs. LOG ON TIME AND LOG THICKNESS vs. LOG ON TIME FOR 66%, 75%, AND 90% DUTY CYCLES

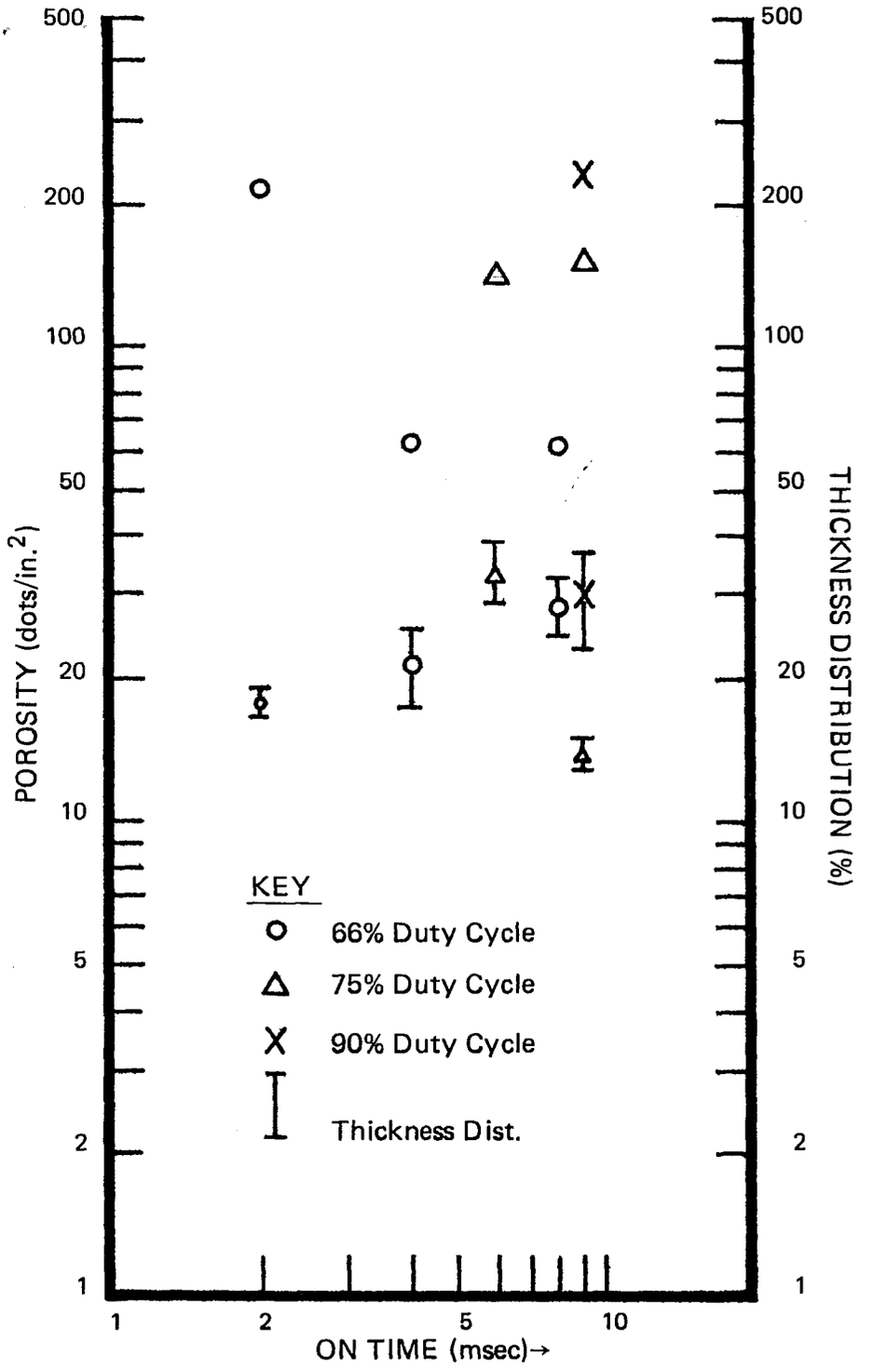

substrate on which the film is deposited. Ashurst and Neale[34] have related pores to foreign matter on the substrate surface. Leeds and Clarke[35-37] categorized porosity from these origins as "inclusion porosity". As described earlier, all deposition-method specimens had ceramic substrates of similar surface finish. The micrograph in Figure 7 shows a representative ceramic surface at 5000X. The evaporated specimens were not removed from the vacuum chamber during deposition of the film system, therefore, contamination from atmospheric particulate fallout was eliminated. Following copper evaporation the specimens which were to be electroplated were placed in clean boxes to minimize any porosity resulting from particulate contamination. A micrograph of the copper film at a magnification of 5000X is shown in Figure 8. The copper has a grain texture similar to that of the ceramic substrate. This was also found to be the case with the very thin films of titanium and palladium which were sandwiched between the copper and the ceramic substrate. Both surface defect concentration and particulate contamination were kept comparable and minimal. "Inclusion porosity" [35-37] was thus held relatively constant while the effect of the deposition method on porosity was observed. A second category Leeds and Clarke [35-37] discussed is "crystallographic porosity". This latter category concerns porosity resulting from structure and is particularly pertinent to the thin gold films being considered. The gold microstructures examined are unique to their deposition method. This provides a basis for studying the affect of crystallographic differences on porosity.

Differences in microstructures of the gold films were observed using scanning electron microscopy. The evaporated film (Figure 9) contains larger diameter grains than the copper underlayer. The grain boundaries are distinct and well defined. The D.C. plated film (Figure 10) shows similar graininess, but with intergranular growth i.e. coalescence not apparent in the evaporated film. In addition grains of smaller size are present between larger grains. Gaps at grain boundaries are thus reduced in D.C. plated, compared to

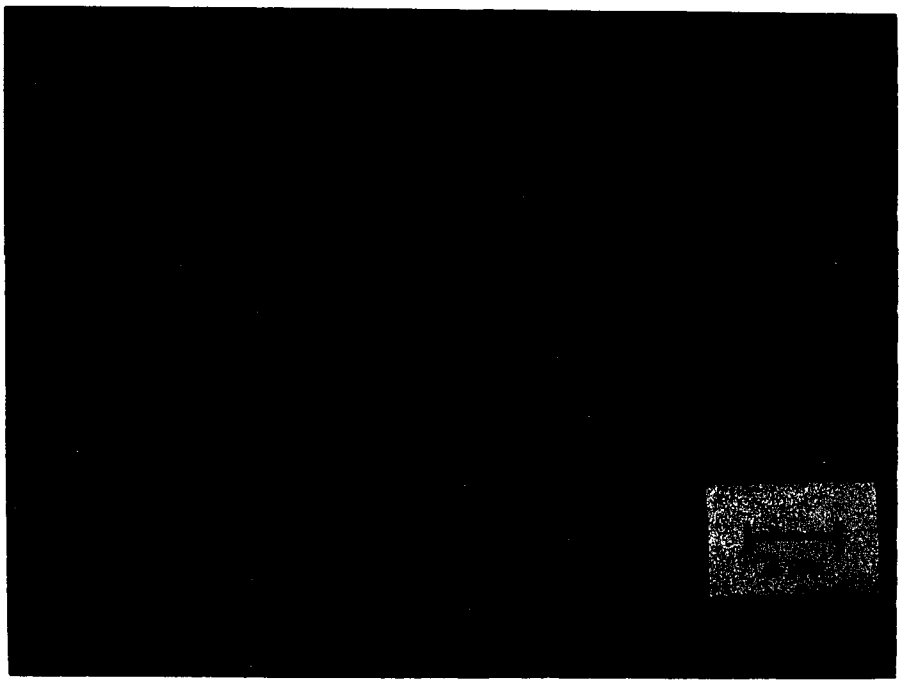

FIG. 7 HIGH ALUMINA CERAMIC, 5000X

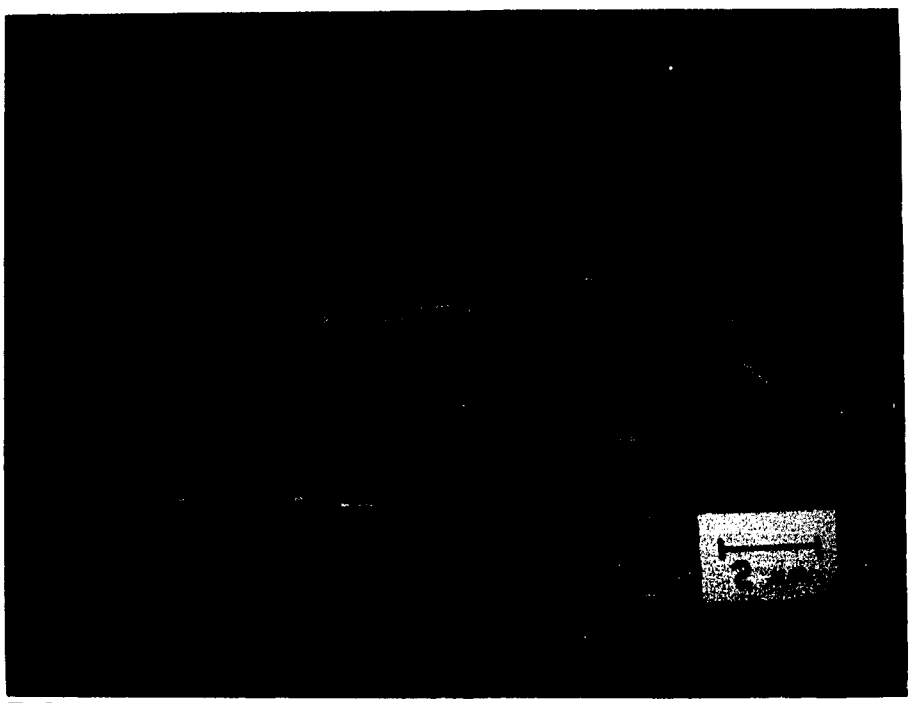

FIG. 8 COPPER UNDERLAYER, 5000X

FIG. 9 EVAPORATED Au, 5000X

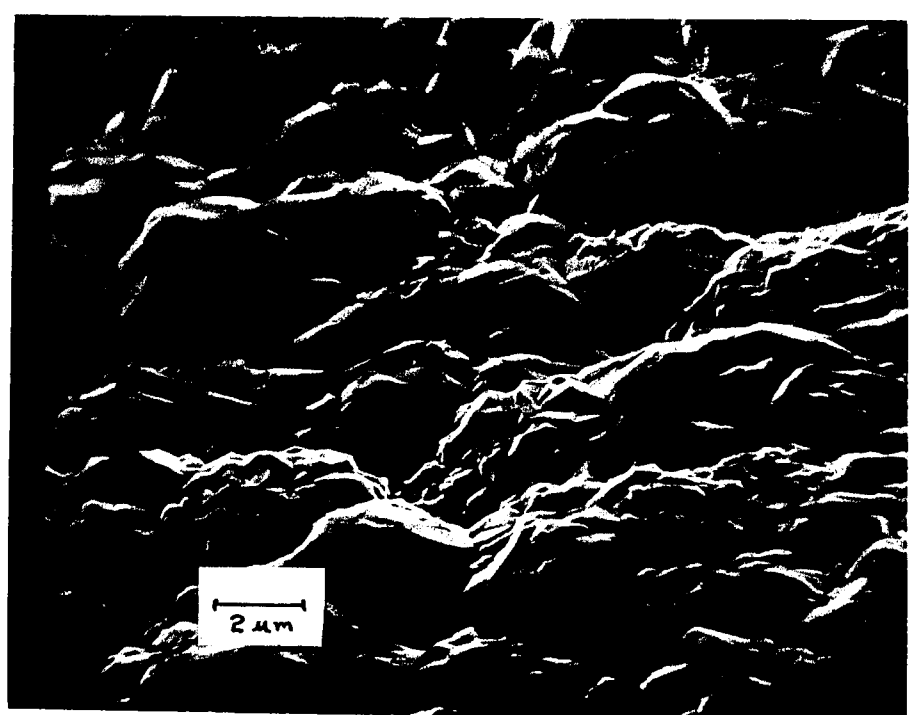

FIG. 10 D. C. PLATED Au, 5000X

evaporated films, by the packing of boundaries with smaller grains and intergranular coalescence.

Asymmetric A.C. plated films (Figure 11) manifest even greater intergranular growth, grain boundaries are virtually indistinguishable. A continuous film with sharply peaked nodules surrounded by cavities is apparent at higher magnification (Figure 12). This topography could result from deplating during the reverse current portion of the A.C. cycle. The pulse plated films (Figure 13), the least porous of those investigated, similarly show a densely packed, continuous film with a high degree of intergranular growth. Distinct large grains and their associated boundaries are barely discernible. Smaller grains coat the surface.

The microstructures of these films indicate that porosity differences are related to the discontinuity at grain boundaries. Just as grain boundaries provide high diffusivity paths in metallic diffusion, they are capable of providing paths of high diffusivity in the chemical penetration of metallic films. The evaporated gold appears to nucleate on the surface and grow into distinct, large grains with well defined boundaries. The plated films show greater intergranular growth, reducing the boundary discontinuity. Grain boundary continuity is accentuated most in the pulse plated films where each pulse provides an increasing probability for nucleation of additional grains. Smaller grains proliferate and provide a densely packed surface. D.C. plating has continuous grain growth with a low density of nucleation sites established in the early stages of film growth. Coalescence, however, reduces grain boundary discontinuity relative to the evaporated films.

The asymmetric A.C. plating which pulses deposition at a frequency of 60 cycles per second, is a variation of the pulse plating method. It similarly provides a continuous probability of nucleation of additional grains.These films have fine grain size lacking grain boundary definition but exhibiting irregular surfaces. The roughness suggests that a less

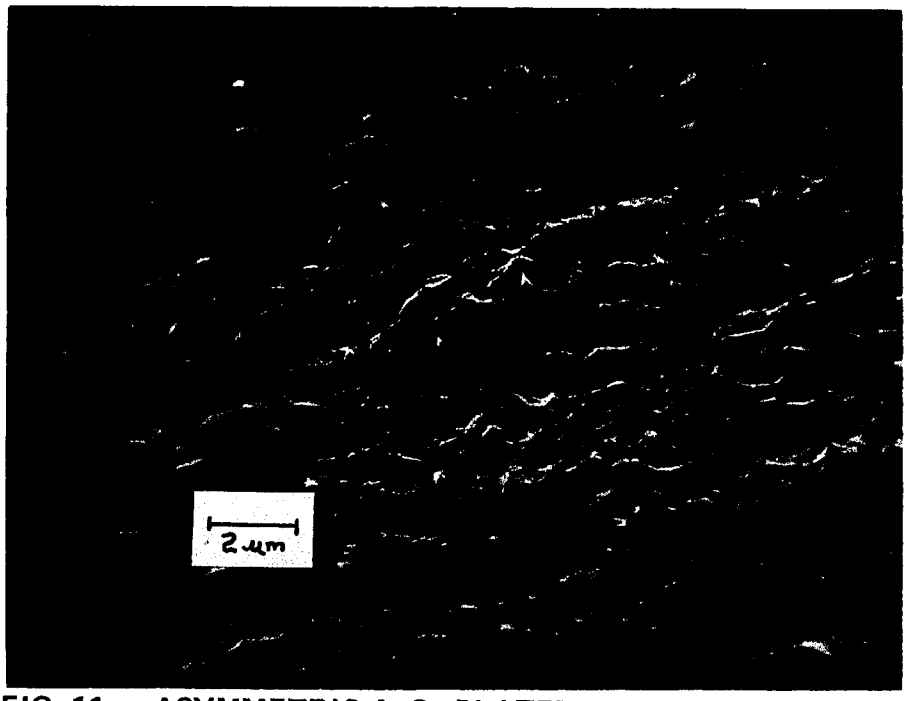

FIG. 11 ASYMMETRIC A. C. PLATED Au,5000X

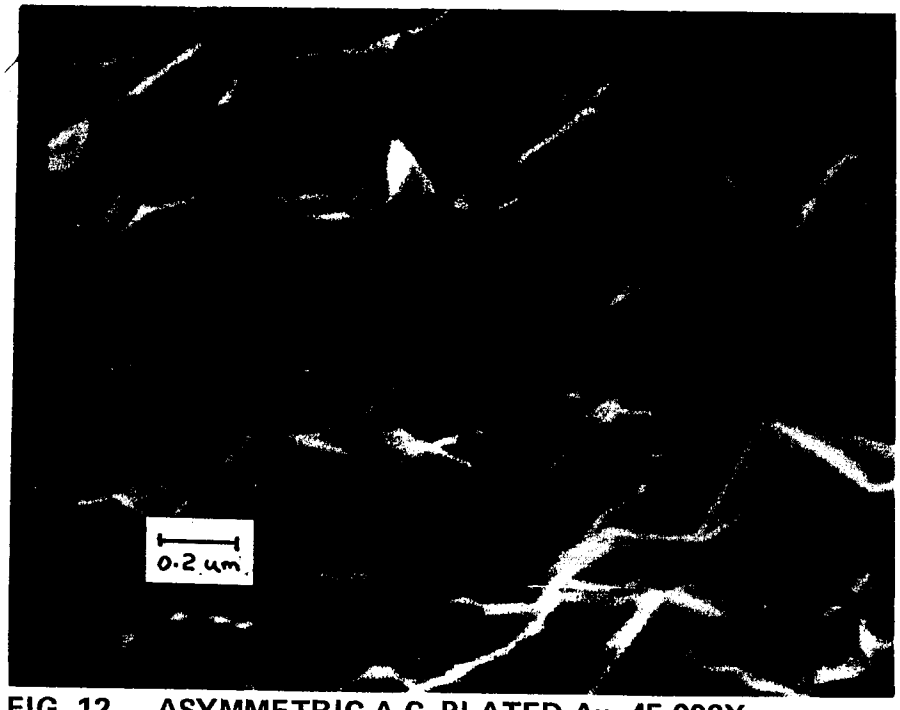

FIG. 12 ASYMMETRIC A.C. PLATED Au, 45,000X SHOWING PEAKED GRAINS

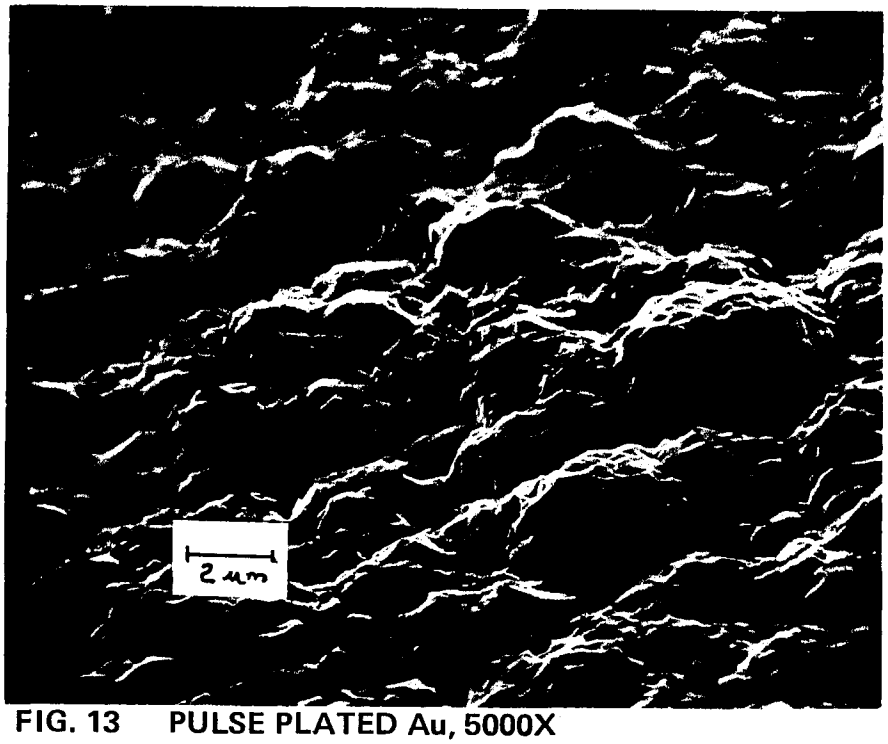

FIG. 13 PULSE PLATED Au, 5000X

dense film is being formed than in pulse plating. As cavities and peaks are overplated, voids could be left unfilled in low lying cavities.

Summary

Pulse plating produced gold films with the least porosity. The porosity of thin gold films is dependent on the method of deposition. Evaporated films are significantly more porous than plated films. Films deposited by D.C. plating, pulse plating, and asymmetric A.C. plating exhibit differing dependencies of porosity on thickness. Scanning electron microscopy studies indicate that porosity in gold thin films is reduced in those deposits with intergranular growth and coalesced grain boundaries, such as the pulse plated films. The variation of pulse waveform produced slight differences in the porosity. A tendency toward a maximum porosity in the 1 to 2 msec ON time range was observed. The variation in pulse waveform produced differences in porosity associated with thickness distribution when examined at low duty cycles i.e. 9% and 33%. At 50% duty cycle, porosity increased with ON time. At longer duty cycles i.e. 66%, 75% and 90% correlations with ON time and thickness distributions could not be made.

III. Thickness Uniformity

A. Introduction

In the most recent review of pulse electroplating[14] the statement is made: "It is generally believed that pulsed plating can lead to a more uniform metal distribution. However, to our knowledge, no systematic investigation has ever been made." Uniformity is an important consideration in the blanket electrodeposition of gold for thin film circuits. Gold films are deposited to a nominal thickness of 4 to 6 microns to assure adequate coverage. An understanding of the uniformity is necessary to minimize excess gold usage and to establish etching times for subsequent process steps where gold is selectively removed. A study was designed with the purpose of measuring the effect of the pulse waveform on thickness uniformity.

B. Procedure

Specimens were prepared according to the procedure in Appendix A at the 30 sets of conditions in Table 1. Two samples at each condition were deposited. One inch diameter disks were punched from the four corners and the center of each sample.

The thickness of each disk was determined by x-ray fluorescence spectroscopy. The number of x-ray counts over a 40 second period at Au_L line were taken for standards of known thickness. A plot of x-ray counts versus thickness was established from the standards. After x-ray counts were taken on the sample, the thickness was taken directly from the calibration plot. Reproducibility within 200 Å is obtainable by this method.

C. Results

The five thicknesses for each sample were recorded, e.g. C for center, TL for top left, LL for lower left and so forth. The differences between the corner thicknesses and the center were also determined e.g. TL - C = ΔTL.

The mean of the four differences was then calculated i.e.

$$\frac{|\Delta TL| + |\Delta TR| + |\Delta LL| + |\Delta LR|}{4} = |\bar{\Delta}|$$

Finally the mean was ratioed to the center thickness and the percent thickness distribution, $\%\bar{\Delta}$, determined:

$$\frac{|\Delta|}{C} \times 100 = \%\bar{\Delta}$$

The average thickness distribution, Ave. $\%\bar{\Delta}$, for each set of samples is listed in the last column of Table 2.

D. Discussion

The thickness distribution measurements are plotted on the same sets of coordinates as porosity as a function of ON time (Figures 3-6). These log thickness distribution vs. log ON time plots do not exhibit a specific trend. At low duty cycles i.e. 9% and 33% thickness distribution reaches a maximum in the ON time range between 0.5 and 2 msec. In the case of the 50% duty cycle distribution tends to increase with ON time. At longer duty cycles patterns in distribution with ON time were not apparent. The average thickness distribution of the D.C. plated specimens was 16.1%, lower than 4 of 5 pulse plated specimens. The latter ranged in distribution from 12.7% at 8 msec ON, 50% duty cycle to 40.3% at 1 msec ON, 9% duty cycle.

The conjecture that thickness distribution would be less with pulse deposition than with D.C. deposition is principled on electrochemical circuitry described in the waveform section.[54] A capacitative layer is formed at the cathode interface. If discharge of this layer resulted in a significant level of metal deposition, pulse plating would produce a more uniform deposit than D.C. plating. Conceptually, pulse plating discharges the capacitance layer during the OFF portion of each cycle. This layer is assumed to be uniform, and discharge results in a uniform secondary current which would effect deposit of a uniform

TABLE 2 THICKNESS DISTRIBUTION (Microns)

NO.	DUTY CYCLE	ON-OFF TIME	TL	TR	C	LL	LR	ΔTL	ΔTR	ΔLL	ΔLR	$\overline{\lvert\Delta\rvert}$	$\overline{\%\Delta}$	Ave $\overline{\%\Delta}$
1	9%	0.1-1.0	2.955	3.311	2.571	3.197	3.782	0.384	0.740	0.626	1.211	0.740	28.8	
2	9%	0.1-1.0	3.332	4.362	2.644	3.958	3.740	0.688	1.708	1.314	1.096	1.202	45.4	37.1
3	9%	0.3-3.0	3.345	3.312	2.913	2.748	3.803	0.432	0.339	-0.155	0.890	0.472	16.2	
4	9%	0.3-3.0	3.443	3.715	3.013	3.405	4.270	0.430	0.712	0.312	1.257	0.695	23.1	19.6
5	9%	0.5-5.0	3.080	3.702	2.841	2.913	3.961	0.239	0.861	0.072	1.120	0.573	20.2	
6	9%	0.5-5.0	3.430	3.585	2.987	3.658	3.847	0.761	0.603	0.676	0.863	0.726	24.3	22.3
7	9%	0.7-7.0	3.114	3.412	2.557	2.866	3.686	0.557	0.855	0.309	1.129	0.713	27.9	
8	9%	0.7-7.0	3.328	3.378	2.731	3.840	3.858	0.597	0.697	1.109	1.127	0.870	31.9	29.9
9	9%	0.9-9.0	3.763	4.288	2.928	2.521	2.570	0.835	1.360	-0.407	-0.358	0.531	18.1	
10	9%	0.9-9.0	3.511	3.228	2.898	3.231	4.028	0.613	0.330	0.333	1.130	0.602	20.8	19.5
11	9%	2.0-10.0	3.449	3.973	2.384	3.247	3.597	1.065	1.589	0.863	1.213	1.183	49.6	
12	9%	2.0-10.0	3.999	3.644	2.854	3.174	4.132	1.145	0.790	0.320	1.278	0.883	30.9	40.3
13	9%	2.0-20.0	3.782	3.299	2.463	3.581	3.266	1.319	0.766	1.118	0.803	1.002	40.7	
14	9%	2.0-20.0	4.010	3.642	2.748	3.377	3.573	1.262	0.894	0.629	0.825	0.903	32.9	36.8
15	9%	4.0-40.0	3.096	3.753	2.682	2.841	3.585	0.414	1.071	0.159	0.903	0.637	23.8	
16	9%	4.0-40.0	3.782	3.594	2.889	3.416	3.906	0.893	0.705	0.527	1.017	0.654	22.6	23.2
17	9%	6.0-60.0	2.855	3.433	2.799	3.058	3.594	0.056	0.634	0.259	0.795	0.436	15.6	
18	9%	6.0-60.0	3.443	3.411	2.993	3.690	3.994	0.450	0.418	0.697	1.001	0.642	21.5	18.5
19	9%	8.0-80.0	2.993	3.214	2.653	3.243	3.734	0.340	0.561	0.590	1.081	0.496	18.7	
20	9%	8.0-80.0	3.353	3.236	3.027	3.841	3.910	0.326	0.209	0.814	0.883	0.558	18.4	18.6
21	9%	9.0-90.0	2.665	3.093	2.402	3.331	3.309	0.263	0.691	0.929	0.907	0.698	29.0	
22	9%	9.0-90.0	2.846	2.741	2.685	3.288	3.680	0.161	0.056	0.603	0.995	0.454	16.9	22.9

TABLE 2 THICKNESS DISTRIBUTION (CONT'D)

NO.	DUTY CYCLE	ON-OFF TIME	TL	TR	C	LL	LR	ΔTL	ΔTR	ΔLL	ΔLR	$\lvert\bar{\Delta}\rvert$	$\overline{\%\Delta}$	Ave $\overline{\%\Delta}$
23	25%	1.0-3.0	3.290	3.853	2.625	3.258	4.179	0.665	1.228	0.633	1.554	1.020	38.9	
24	25%	1.0-3.0	4.165	4.014	2.923	3.401	4.498	1.242	1.091	0.978	1.575	1.222	41.8	40.3
25	33%	0.5-1.0	3.258	4.100	2.958	3.548	3.899	0.300	1.142	0.590	0.941	0.743	25.1	
26	33%	0.5-1.0	4.508	4.450	3.162	3.539	4.447	1.346	1.288	0.377	1.285	1.074	34.0	29.6
27	33%	1.0-2.0	3.148	3.742	3.140	3.333	3.403	0.008	0.602	0.193	0.263	0.267	8.5	
28	33%	1.0-2.0	3.621	4.058	3.056	4.020	4.792	0.565	1.002	0.964	1.736	1.067	34.9	21.7
29	33%	2.0-4.0	3.382	3.804	3.150	3.399	4.145	0.232	0.654	0.249	0.995	0.533	16.9	
30	33%	2.0-4.0	3.680	3.693	3.240	3.826	4.634	0.440	0.453	0.586	0.394	0.468	14.5	15.7
31	33%	4.0-8.0	3.756	3.795	2.892	3.546	4.247	0.864	0.903	0.654	1.355	0.944	32.6	
32	33%	4.0-8.0	3.480	3.647	3.271	3.878	3.879	0.209	0.376	0.607	0.608	0.450	13.8	23.2
33	33%	6.0-12.0	3.600	3.699	3.166	3.245	4.304	0.434	0.533	0.079	1.138	0.546	17.2	
34	33%	6.0-12.0	3.757	3.675	2.801	3.836	4.110	0.956	0.874	0.035	1.309	0.794	28.3	22.8
35	33%	8.0-16.0	3.634	3.954	3.028	2.926	3.791	0.606	0.926	-0.102	0.763	0.599	19.8	
36	33%	8.0-16.0	3.603	3.343	3.419	3.884	4.396	0.184	-0.076	0.465	0.927	0.413	12.1	15.9
37	33%	9.0-18.0	3.470	4.217	3.002	2.822	3.641	0.468	1.215	-0.180	0.539	0.646	21.5	
38	33%	9.0-18.0	3.639	3.446	3.536	3.604	4.501	0.103	-0.090	0.068	0.965	0.307	8.7	15.1
39	50%	1.0-1.0	3.279	3.784	2.720	3.328	3.964	0.559	1.064	0.608	1.244	0.869	31.9	
40	50%	1.0-1.0	4.718	4.101	3.257	4.081	4.045	1.461	0.844	0.824	0.788	0.979	30.1	31.0
41	50%	2.0-2.0	3.659	3.769	2.882	3.357	3.786	0.777	0.887	0.475	0.904	0.761	26.4	
42	50%	2.0-2.0	3.589	4.099	2.725	3.613	4.335	0.864	1.374	0.888	1.610	1.184	43.4	34.9
43	50%	4.0-4.0	3.550	3.659	3.060	3.010	4.131	0.490	0.599	-0.050	1.071	0.553	18.1	
44	50%	4.0-4.0	3.877	3.517	3.327	3.692	4.684	0.550	0.191	0.365	1.357	0.616	18.5	18.3

TABLE 2 THICKNESS DISTRIBUTION (CONT'D)

NO.	DUTY CYCLE	ON-OFF TIME	TL	TR	C	LL	LR	ΔTL	ΔTR	ΔLL	ΔLR	$\lvert\overline{\Delta}\rvert$	$\overline{\%\Delta}$	Ave $\overline{\%\Delta}$
45	50%	6.0-6.0	3.468	3.641	3.335	3.613	4.002	0.132	0.306	0.278	0.667	0.346	10.4	
46	50%	6.0-6.0	3.780	3.524	3.332	3.724	4.673	0.448	0.192	0.392	1.341	0.593	17.8	14.1
47	50%	8.0-8.0	3.454	3.741	3.297	3.536	4.014	0.157	0.444	0.239	0.717	0.389	11.8	
48	50%	8.0-8.0	3.905	3.467	3.447	3.837	4.752	0.458	0.020	0.390	1.005	0.468	13.6	12.7
49	50%	9.0-9.0	3.572	3.830	3.092	4.017	4.140	0.480	0.738	0.925	1.048	0.798	25.8	
50	50%	9.0-9.0	3.625	3.262	3.464	3.918	4.136	0.161	-0.202	0.504	0.672	0.385	11.1	18.4
51	60%	2.0-1.0	3.373	4.505	3.077	2.874	3.319	0.296	1.428	-0.213	0.242	0.545	17.7	
52	60%	2.0-1.0	3.874	3.207	3.694	3.385	5.221	0.180	0.487	-0.309	1.521	0.626	16.9	17.3
53	60%	4.0-2.0	3.489	4.273	3.019	3.194	3.245	0.470	1.254	0.175	0.226	0.531	17.6	
54	60%	4.0-2.0	3.811	3.413	3.119	3.404	4.968	0.692	0.294	0.285	1.849	0.780	25.0	21.3
55	60%	8.0-4.0	3.527	3.597	2.889	3.333	3.975	0.638	0.708	0.444	1.086	0.719	24.9	
56	60%	8.0-4.0	3.820	3.570	2.909	3.346	4.543	0.911	0.661	0.437	1.636	0.911	31.3	28.1
57	75%	6.0-2.0	3.544	4.241	2.933	3.348	4.047	0.611	1.309	0.415	1.114	0.862	29.4	
58	75%	6.0-2.0	4.548	3.880	2.876	3.346	3.671	1.672	1.004	0.470	0.795	0.985	34.3	31.8
59	75%	9.0-3.0	3.964	3.795	3.035	3.087	3.361	0.429	0.710	0.052	0.336	0.394	13.0	
60	75%	9.0-3.0	3.893	3.085	3.387	3.446	4.531	0.506	-0.302	0.059	1.144	0.503	14.9	13.9
61	90%	9.0-1.0	2.870	4.095	2.539	3.654	3.261	0.331	1.556	1.115	0.722	0.937	36.7	
62	90%	9.0-1.0	3.677	2.715	3.152	3.179	5.048	0.525	-0.437	0.027	1.896	0.721	22.9	29.8
63		D.C.	3.042	3.874	2.714	2.943	2.784	0.328	1.165	0.129	0.070	0.423	15.6	
64		D.C.	3.165	2.980	3.170	3.132	4.816	-0.005	-0.190	-0.038	1.640	0.516	16.3	16.0

metal film. The experimental measurements do not confirm these premises. Less than 20% of the pulse plated samples exhibited lower thickness distribution than D. C. plated samples. Also, the smallest distributions were not found in samples deposited at the highest frequency; high frequency discharge of capacitance would have produced the most uniform deposits if the model described was operative. Experiment does not substantiate this prediction. No basis was found for predicting more uniform deposits on planar surfaces with pulse than with D. C. plated gold. In those cases where pulse deposits were more uniform than D. C. e.g. 12.7% at 8 msec ON, 50% duty cycle; compared to 16.1% at D.C. conditions, the improvement was marginal and within experimental error.

IV. Microstructure

A. Introduction

The scanning electron micrographs used to evaluate the porosity differences among evaporated, asymmetric A.C., D.C. and pulse plated films illustrate the effect of the deposition method on the structure of the gold. A detailed SEM examination of the effects caused by variation of the pulse plated waveform was similarly undertaken. The objective was to determine the effects that variations in duty cycle and ON time have on the morphology of the gold deposits.

B. Specimen Preparation

Specimens were prepared according to the procedure described in Appendix A. Gold films nominally 4 microns thick were examined. The samples were plated at the 30 pulsing conditions listed in Table 1. The average current density was 5 amp/ft^2. This value was choosen since it is near the limiting current density, i.e. the point at which H_2 evolution occurs. Differences in structure were anticipated to be accentuated near the limiting current.

C. Results

The scanning electron micrographs of the pulse plated gold films are shown in Figures 14-41. It was found that as the duty cycle decreased the grain size decreased for films formed with long ON times (i.e. 9 msec, 8 msec, 6 msec, 4 msec ON). This is illustrated by the case at 9 msec ON:

Duty Cycle	ON-OFF Time	Average Grain Size
90%	9.0-1.0 msec	1.8
75%	9.0-3.0 msec	1.4
50%	9.0-9.0 msec	1.0
33%	9.0-18.0 msec	0.8
9%	9.0-90.0 msec	0.6

FIG. 14 Au DEPOSITED AT 9% DUTY CYCLE:
0.1 msec ON, 1 msec OFF; 10,000X

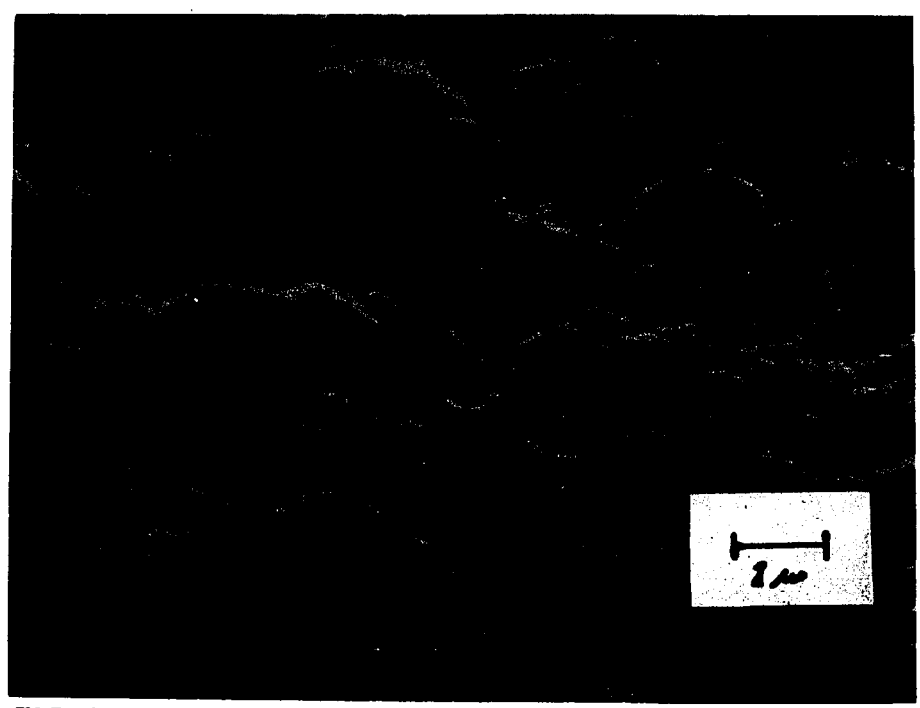

FIG. 15 Au DEPOSITED AT 9% DUTY CYCLE:
0.3 msec ON, 3 msec OFF; 10,000X

FIG. 16 Au DEPOSITED AT 9% DUTY CYCLE:
0.5 msec ON, 5 msec OFF; 10,000X

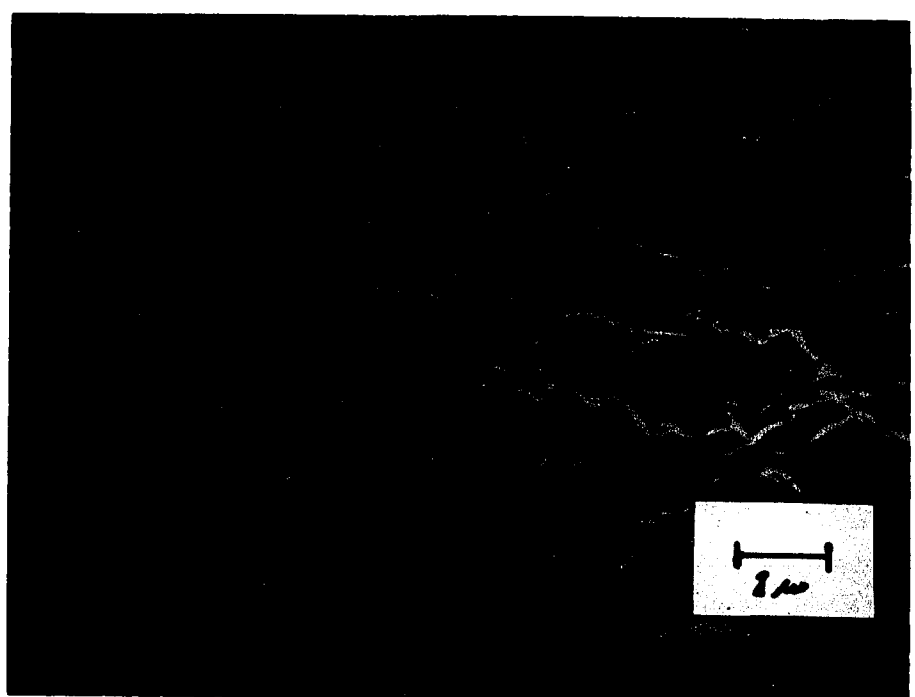

FIG. 17 Au DEPOSITED AT 9% DUTY CYCLE:
0.7 msec ON, 7 msec OFF; 10,000X

FIG. 18 Au DEPOSITED AT 9% DUTY CYCLE:
2.0 msec ON, 20 msec OFF; 10,000X

FIG. 19 Au DEPOSITED AT 9% DUTY CYCLE:
4.0 msec ON, 40 msec OFF; 10,000X

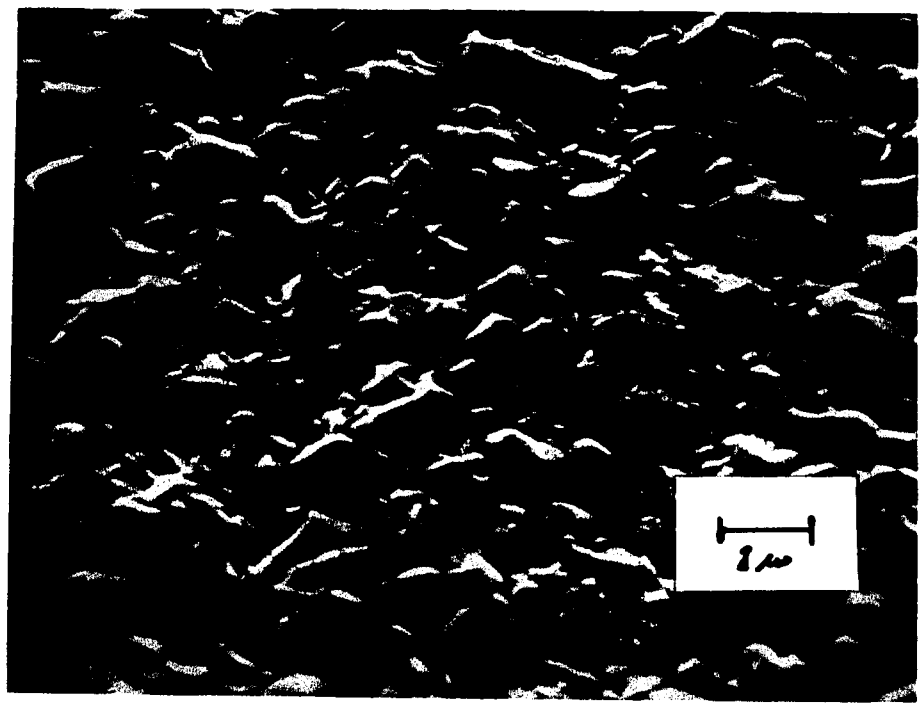

FIG. 20 Au DEPOSITED AT 9% DUTY CYCLE:
6.0 msec ON, 60 msec OFF; 10,000X

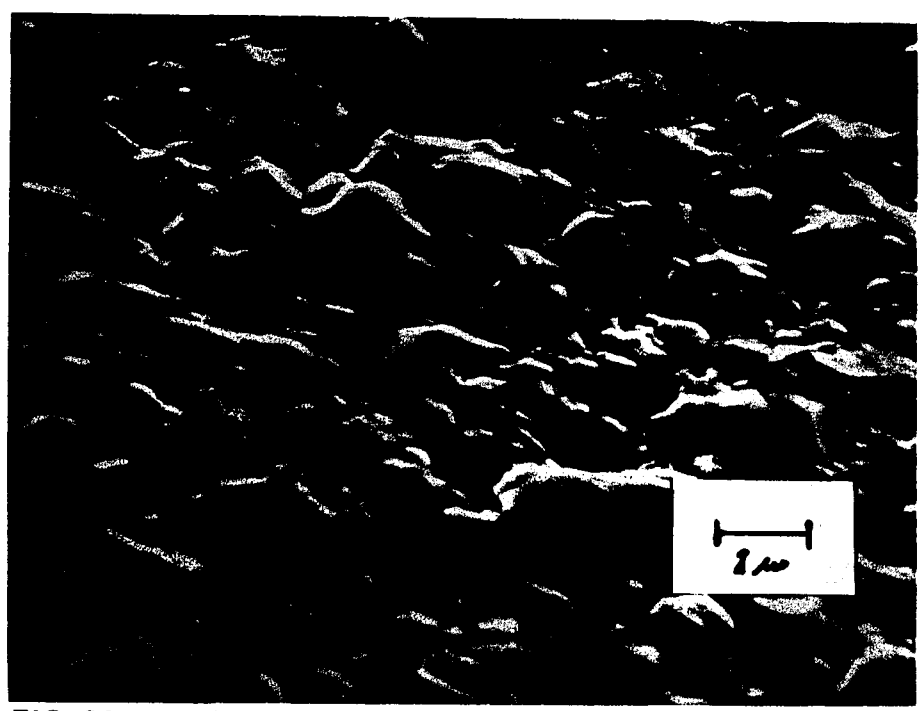

FIG. 21 Au DEPOSITED AT 9% DUTY CYCLE:
8.0 msec ON, 80 msec OFF; 10,000X

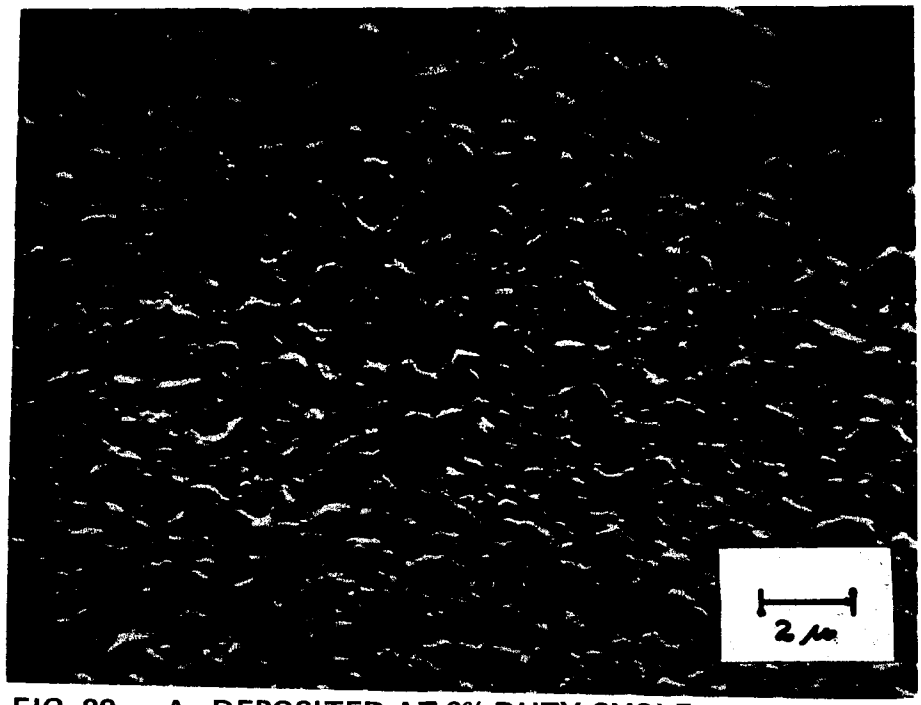

FIG. 22 Au DEPOSITED AT 9% DUTY CYCLE:
9.0 msec ON, 90 msec OFF; 5,000X

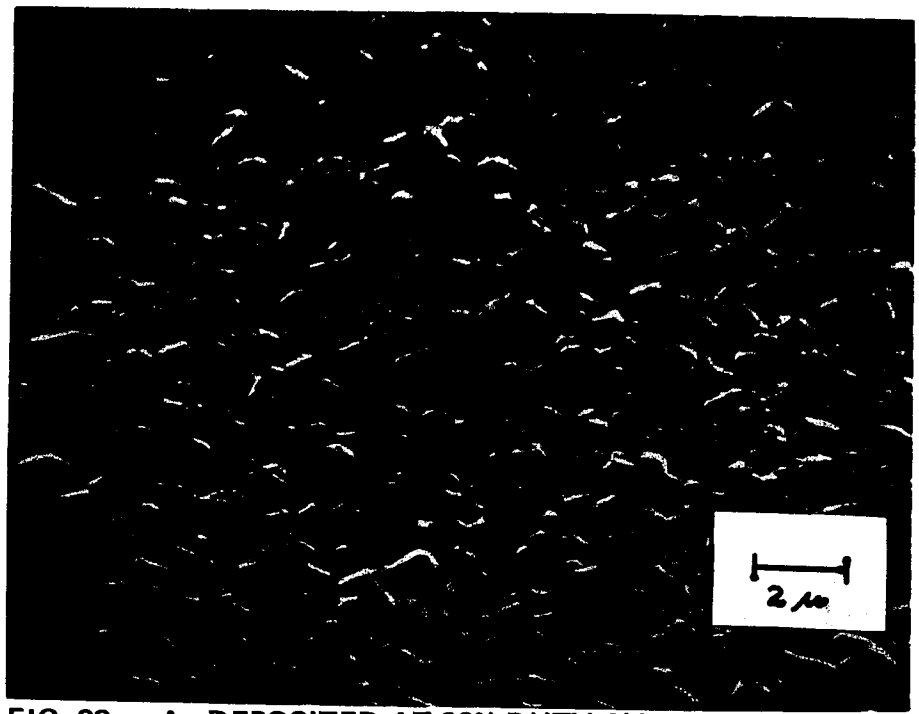

FIG. 23 Au DEPOSITED AT 33% DUTY CYCLE:
9.0 msec ON, 18 msec OFF; 5,000X

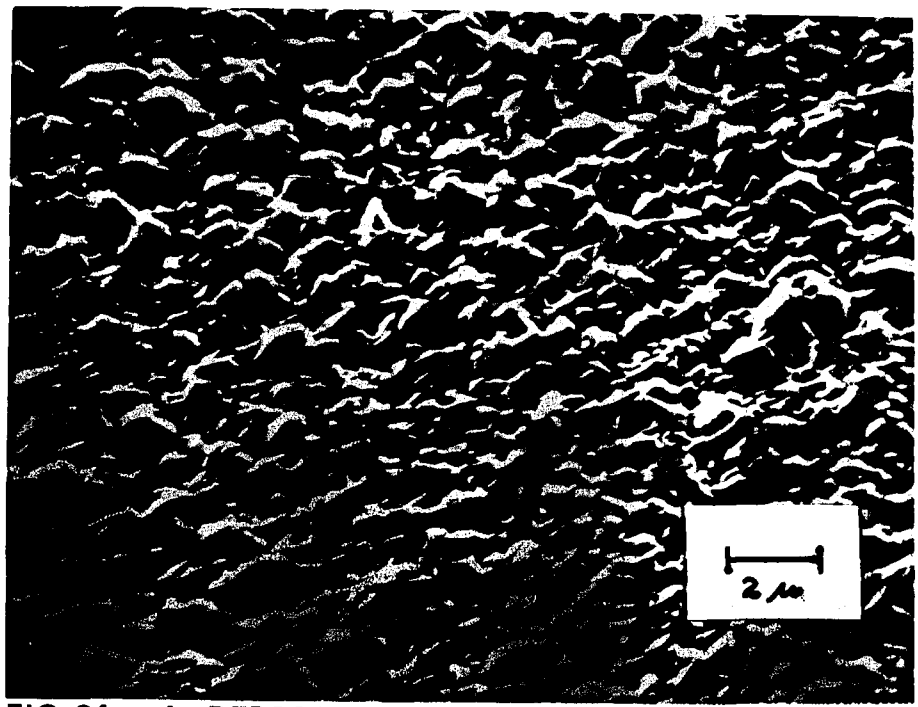

FIG. 24 Au DEPOSITED AT 50% DUTY CYCLE:
9.0 msec ON, 9.0 msec OFF; 5,000X

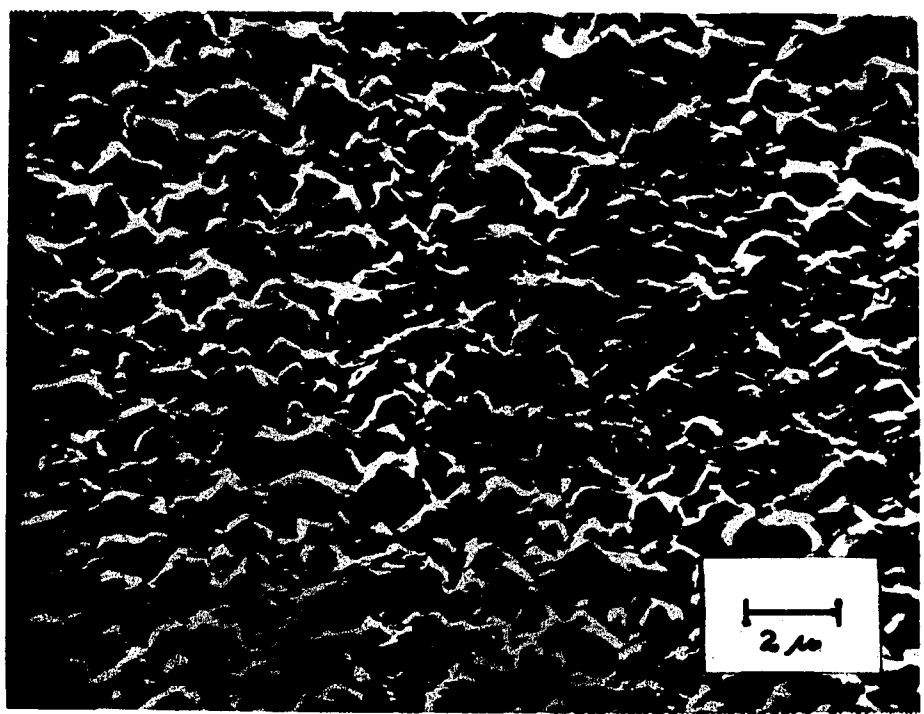

FIG. 25 Au DEPOSITED AT 75% DUTY CYCLE:
9.0 msec ON, 3 msec OFF; 5,000X

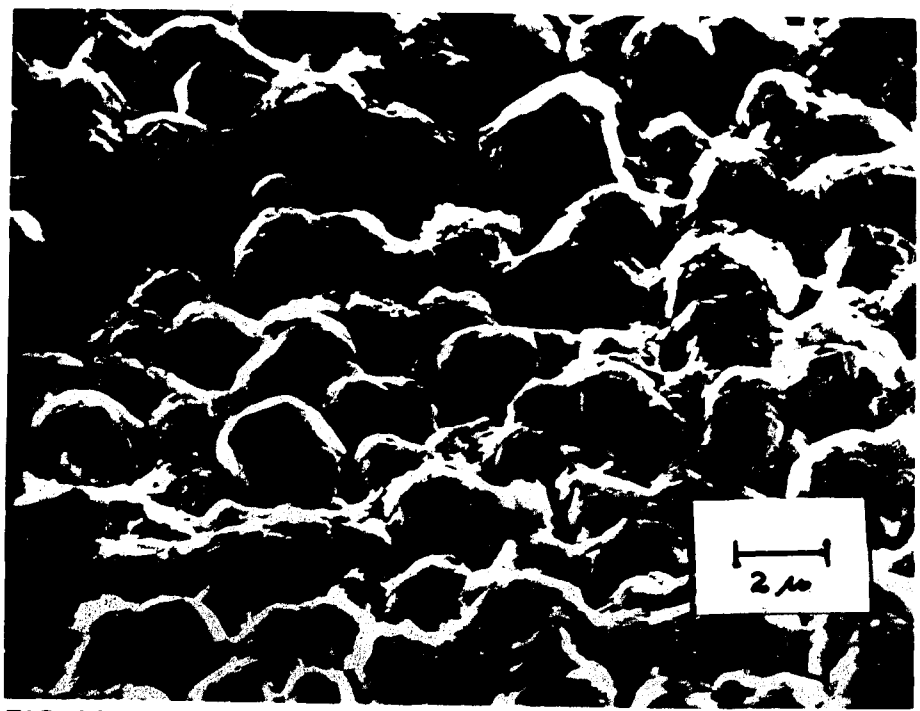

FIG. 26 Au DEPOSITED AT 90% DUTY CYCLE:
9.0 msec ON, 1 msec OFF; 5,000X

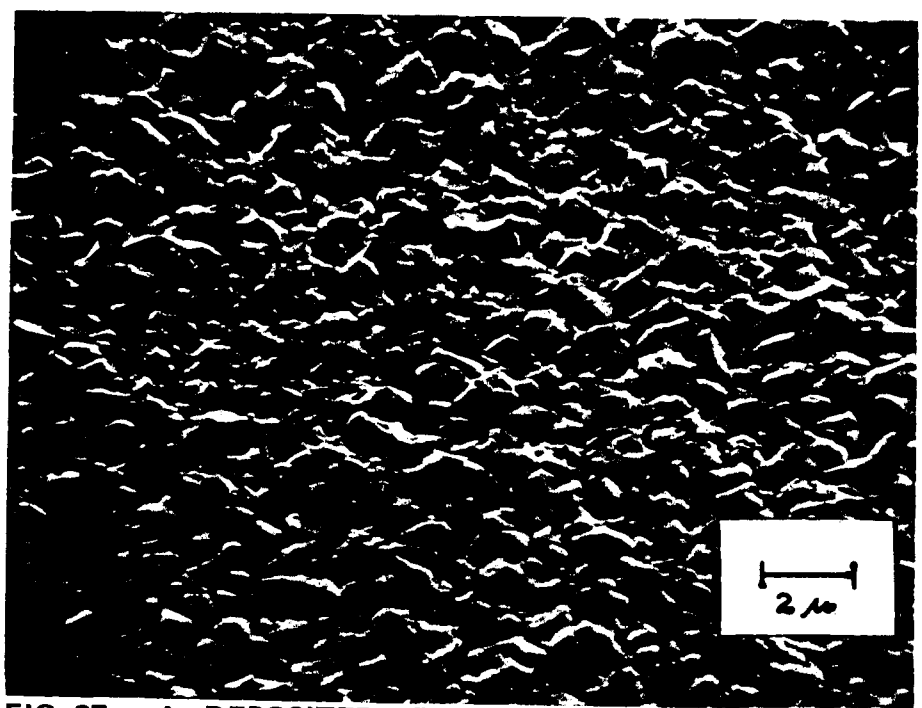

FIG. 27 Au DEPOSITED AT 33% DUTY CYCLE:
8.0 msec ON, 16 msec OFF; 5,000X

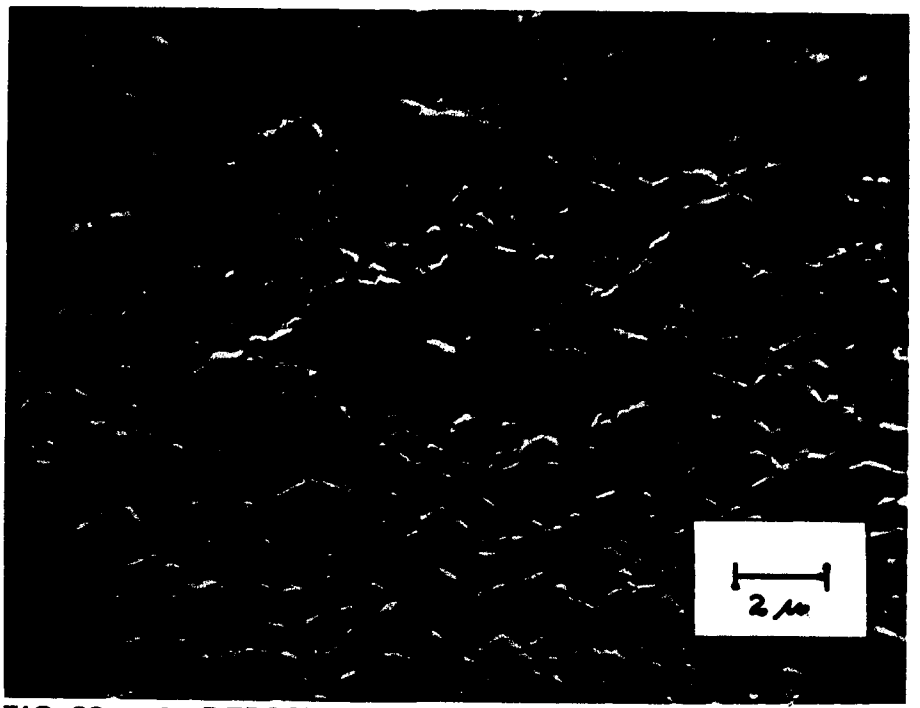

FIG. 28 Au DEPOSITED AT 50% DUTY CYCLE:
8.0 msec ON, 8 msec OFF; 5,000X

FIG. 29 Au DEPOSITED AT 66% DUTY CYCLE:
8.0 msec ON, 4 msec OFF; 5,000X

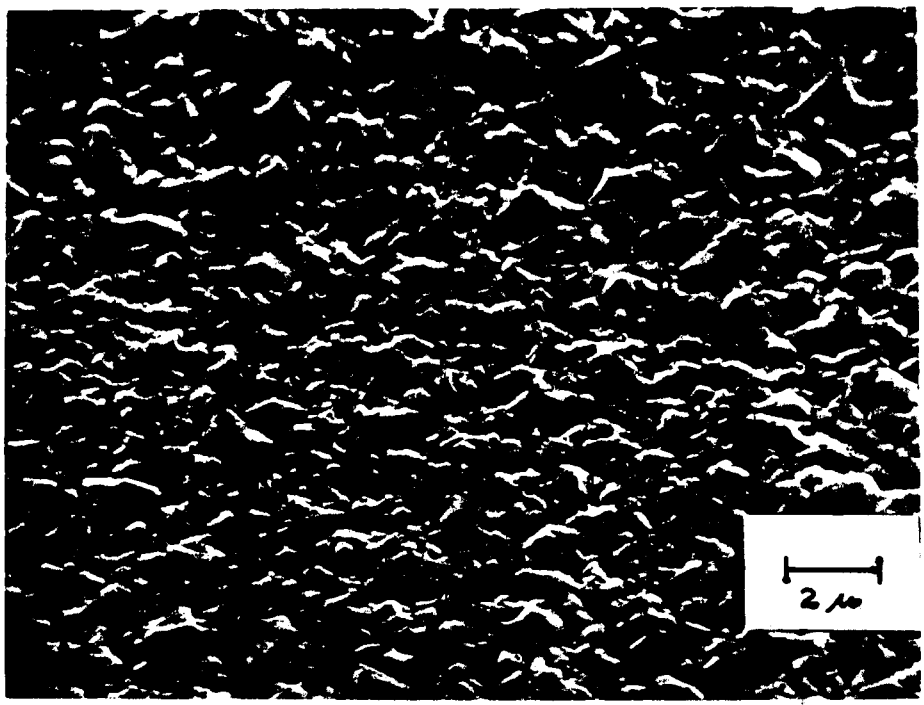

FIG. 30 Au DEPOSITED AT 33% DUTY CYCLE:
6.0 msec ON, 12 msec OFF; 5,000X

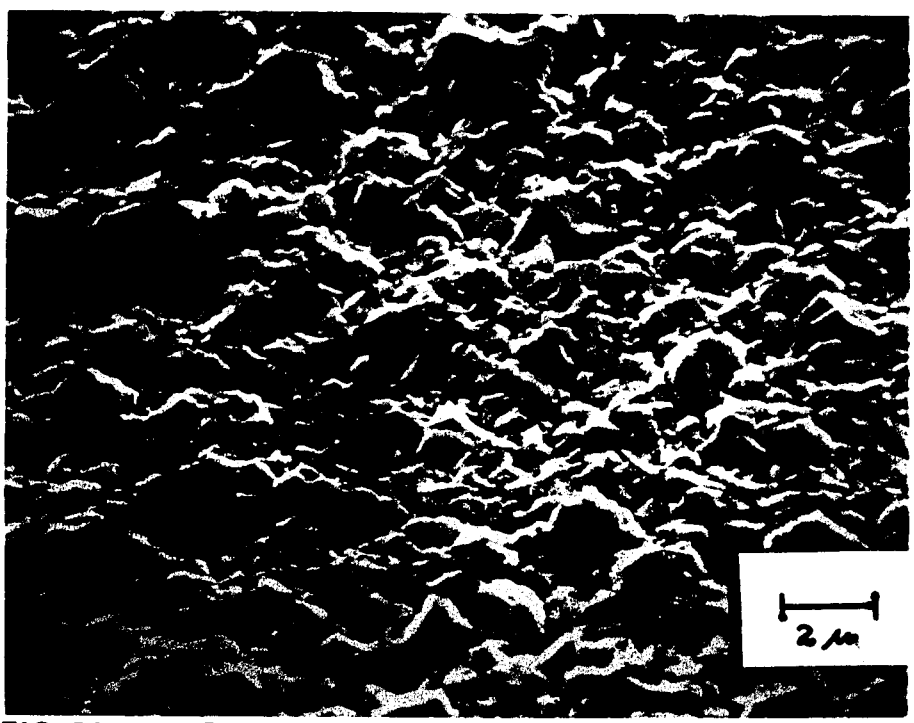

FIG. 31 Au DEPOSITED AT 50% DUTY CYCLE:
6.0 msec ON, 6 msec OFF; 5,000X

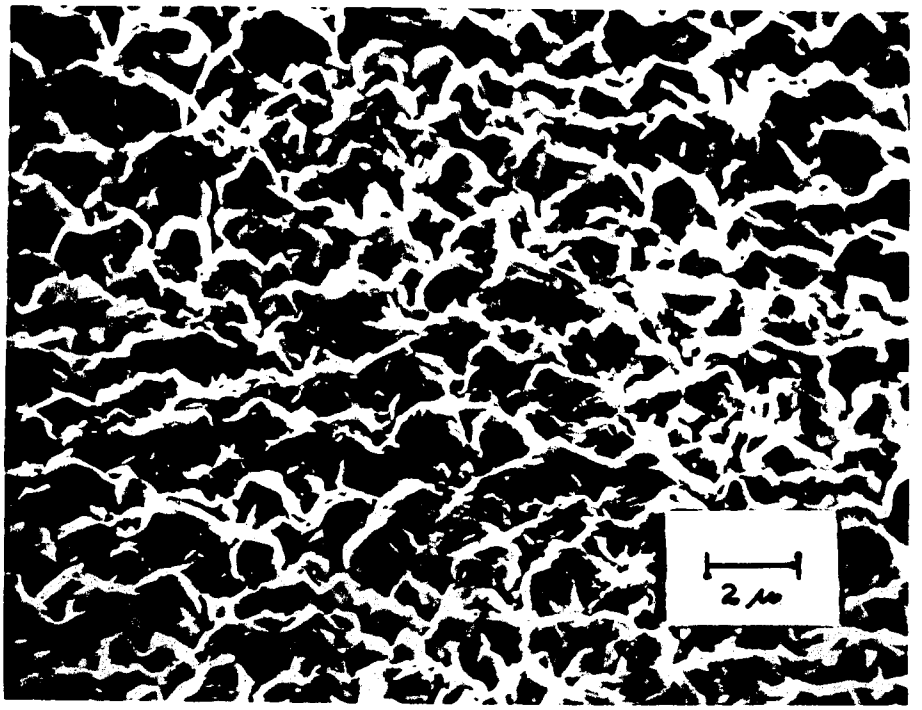

FIG. 32 Au DEPOSITED AT 75% DUTY CYCLE:
6.0 msec ON, 2 msec OFF; 5,000X

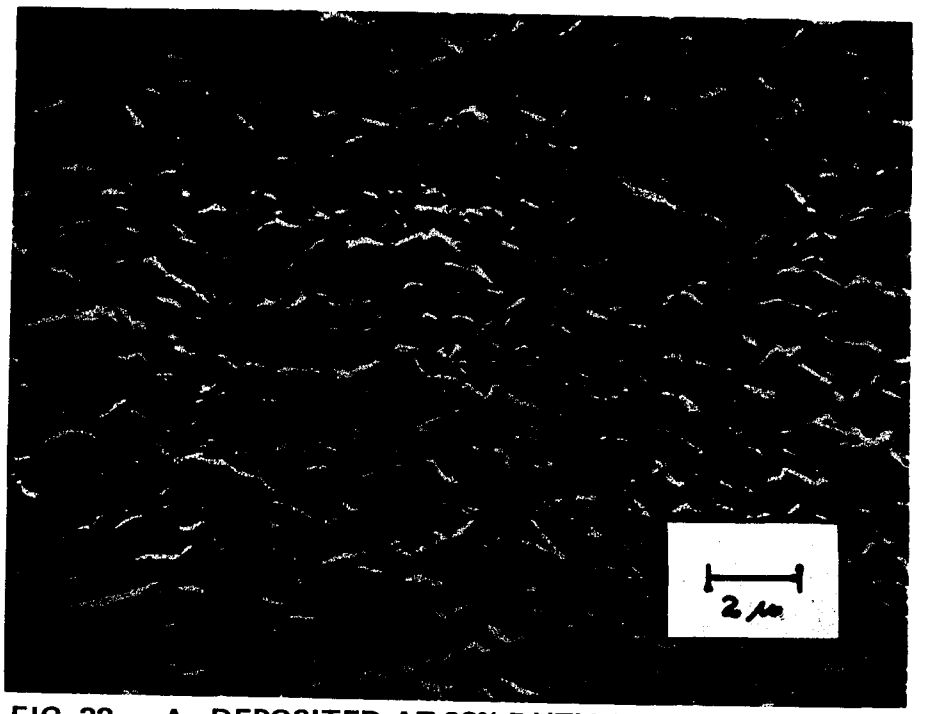

FIG. 33 Au DEPOSITED AT 33% DUTY CYCLE:
4.0 msec ON, 8 msec OFF; 5,000X

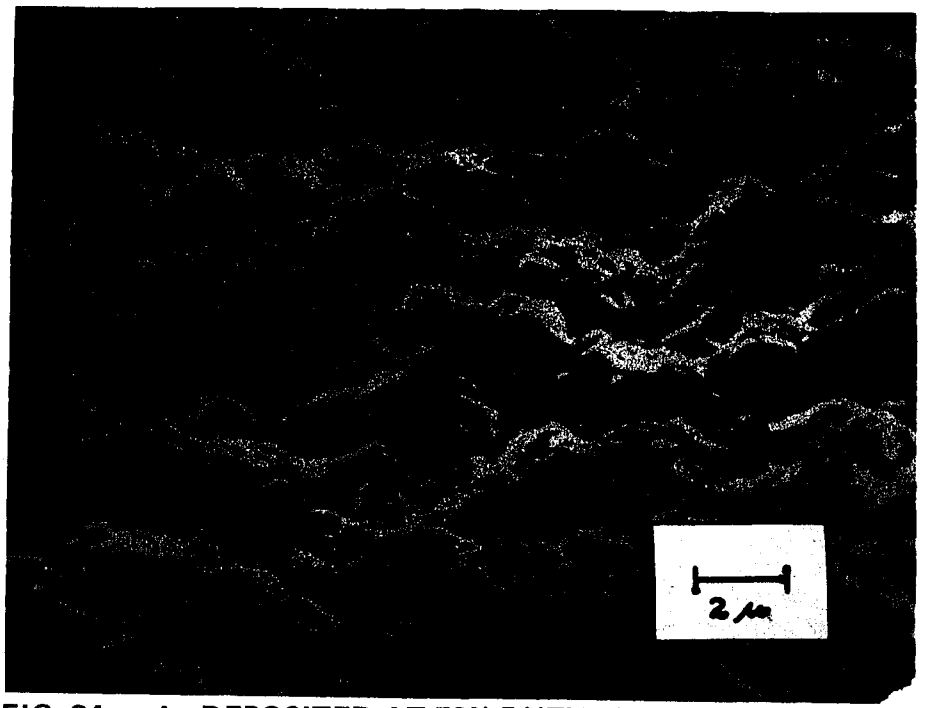

FIG. 34 Au DEPOSITED AT 50% DUTY CYCLE:
4.0 msec ON, 4 msec OFF; 5,000X

FIG. 35 Au DEPOSITED AT 66% DUTY CYCLE:
4.0 msec ON, 2 msec OFF; 5,000X

FIG. 36 Au DEPOSITED AT 33% DUTY CYCLE:
2.0 msec ON, 4 msec OFF; 5,000X

FIG. 37 Au DEPOSITED AT 50% DUTY CYCLE:
2.0 msec ON, 2 msec OFF; 5,000X

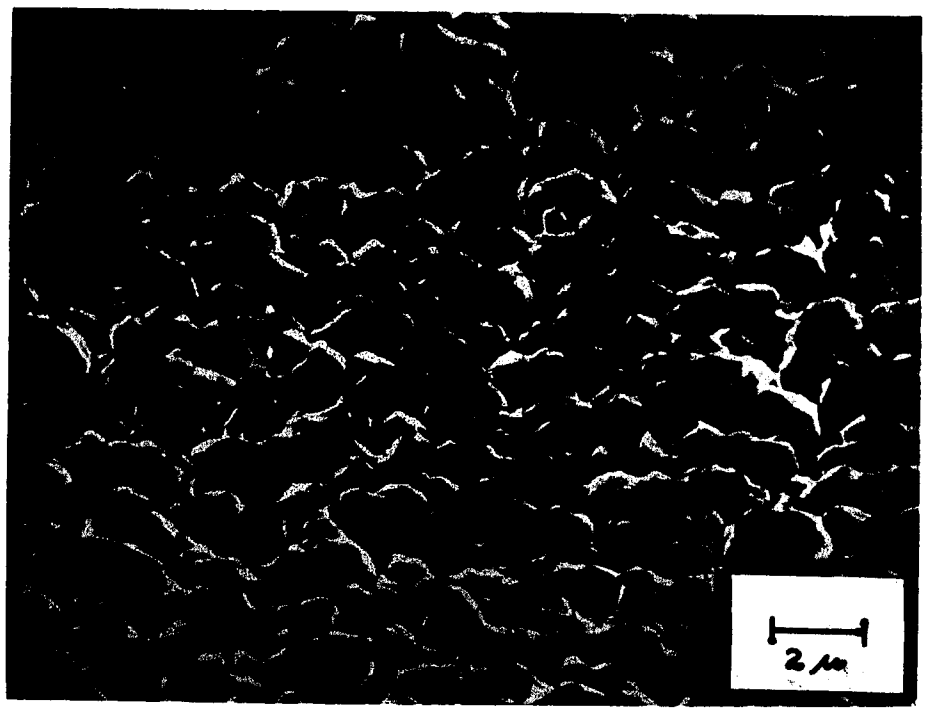

FIG. 38 Au DEPOSITED AT 66% DUTY CYCLE:
2 msec ON, 1 msec OFF; 5,000X

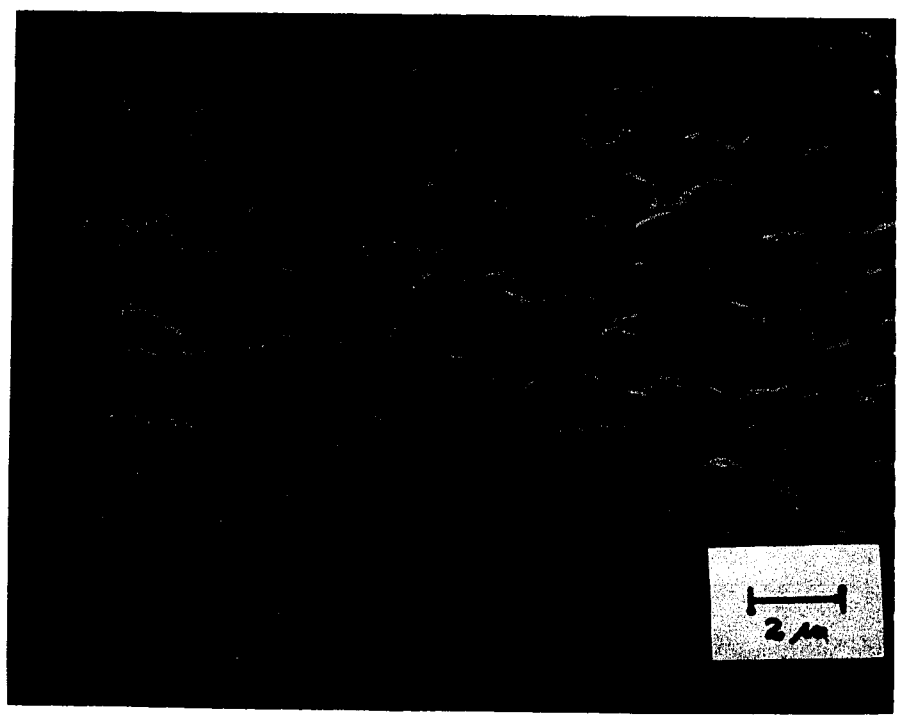

FIG. 39 Au DEPOSITED AT 25% DUTY CYCLE:
1 msec ON, 3 msec OFF; 5,000X

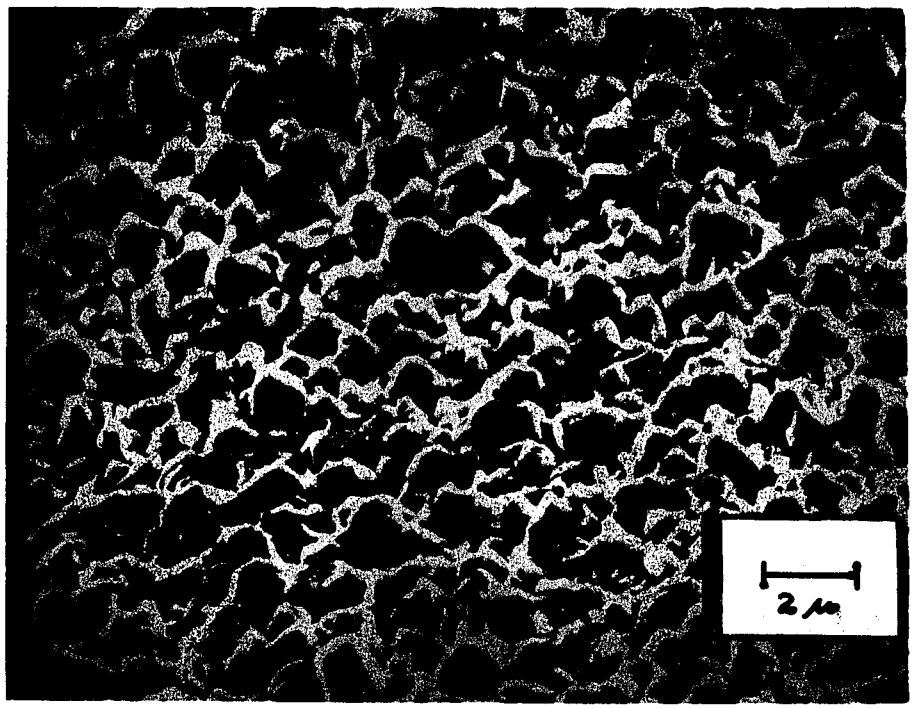

FIG. 40 Au DEPOSITED AT 33% DUTY CYCLE:
1 msec ON, 2 msec OFF; 5,000X

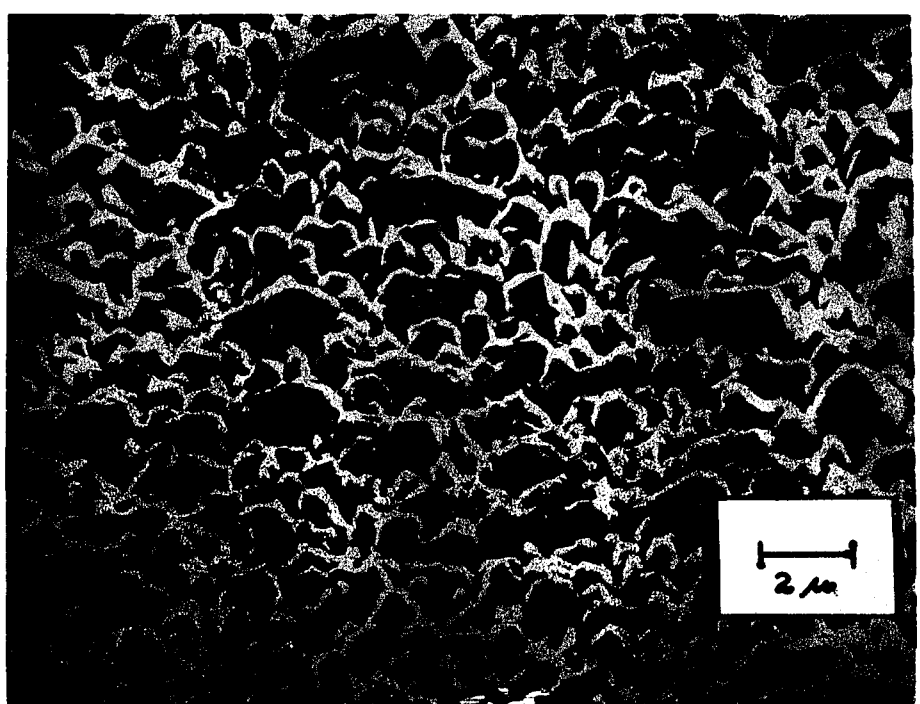

FIG. 41 Au DEPOSITED AT 50% DUTY CYCLE:
1 msec ON, 1 msec OFF; 5,000X

At 2 msec ON the variation of OFF time does not produce this change in grain size. As the ON time decreases within a given duty cycle the grain size increases to 2 msec ON, then becomes reasonably constant at ON times less than 2 msec.

D. Discussion

The microstructures of the deposits formed by various waveforms have differences in grain size. The pattern of increased grain size with duty cycle is presumed to be related to the rate of cation impingement. It should be noted that the total impingement was constant for all samples since they were all produced at the same average current density. The instantaneous impingement rate, however, is proportional to peak current density, which varied. This is highest for the shortest duty cycles.

At short duty cycles the maximum number of nucleation sites are generated. Bockris and Damjanovic[38] have shown the rate of nucleation, R, can be considered by the following expression:

$$R = 2\pi r_c n^2 \left(\frac{kT}{2\pi m}\right)^{1/2} \exp\left[-\frac{\Delta F_c + E}{kT}\right]$$

r_c = critical radius of the nucleus

n = no. of adions/cm^2

ΔF_c = free energy change for formation of the nucleus

E = activation energy for surface diffusion

The critical nucleus is given by:

$$r_c = \frac{\sqrt{3}}{2} \frac{d^2\Upsilon}{kT \ln c/c_o}$$

Υ = edge energy of the nucleus

d = interatomic distance

c = adion concentration in electric field

c_o = adion concentration without electric field

The radius of the critical nucleus is defined as the radius of a cluster of atoms, with which an additional atom would have a 50% probability of stability.

The rate of nucleation, R, is maximized when the adion concentration is greatest. Adion concentration, n, is at a maximum when cation impingement is greatest. The critical radius is inversely proportional to the log of the adion concentration in the electric field, ln c. The critical nucleus size is thus minimized when cation impingement is maximized. Since the cation impingement rate is highest at the shortest duty cycle, the rate of nucleation is highest and the critical nucleus is smallest with short duty cycle waveforms. This situation produces the smallest size and greatest number of grains per area.

When the solvated cations in solution impinge upon the polarization layer at the electrode interface, (Figure 42), they lose some of their water of hydration and become adsorbed on the substrate surface as adions. After the initial aggregation of nucleation sites, arriving adions diffuse across the surface to the established nuclei. Remaining adion hydration is removed in a series of steps as the adion diffuses along the nucleation site. When the adion reaches its most energetically stable position, it is incorporated in the nucleus and charge transfer occurs.[39] The grain continues to build on the established nuclei.

The nuclei enlarge their radii until the substrate surface is coated with adjoining nuclei. Grains then grow normal to the surface on the foundation of the previously formed nucleation centers. First, growth occurs most persistently, i.e. with minimum interruption, with waveforms of long ON time.

The longer the ON time, the more complete is the surface coverage by nucleation during the first pulse. Within a set of ON times at a given duty cycle, the probability of secondary nucleation following the first pulse diminished with increasing ON time. This is a result of the increased initial surface coverage.

FIG. 42: CATHODE-ELECTROLYTE INTERFACE

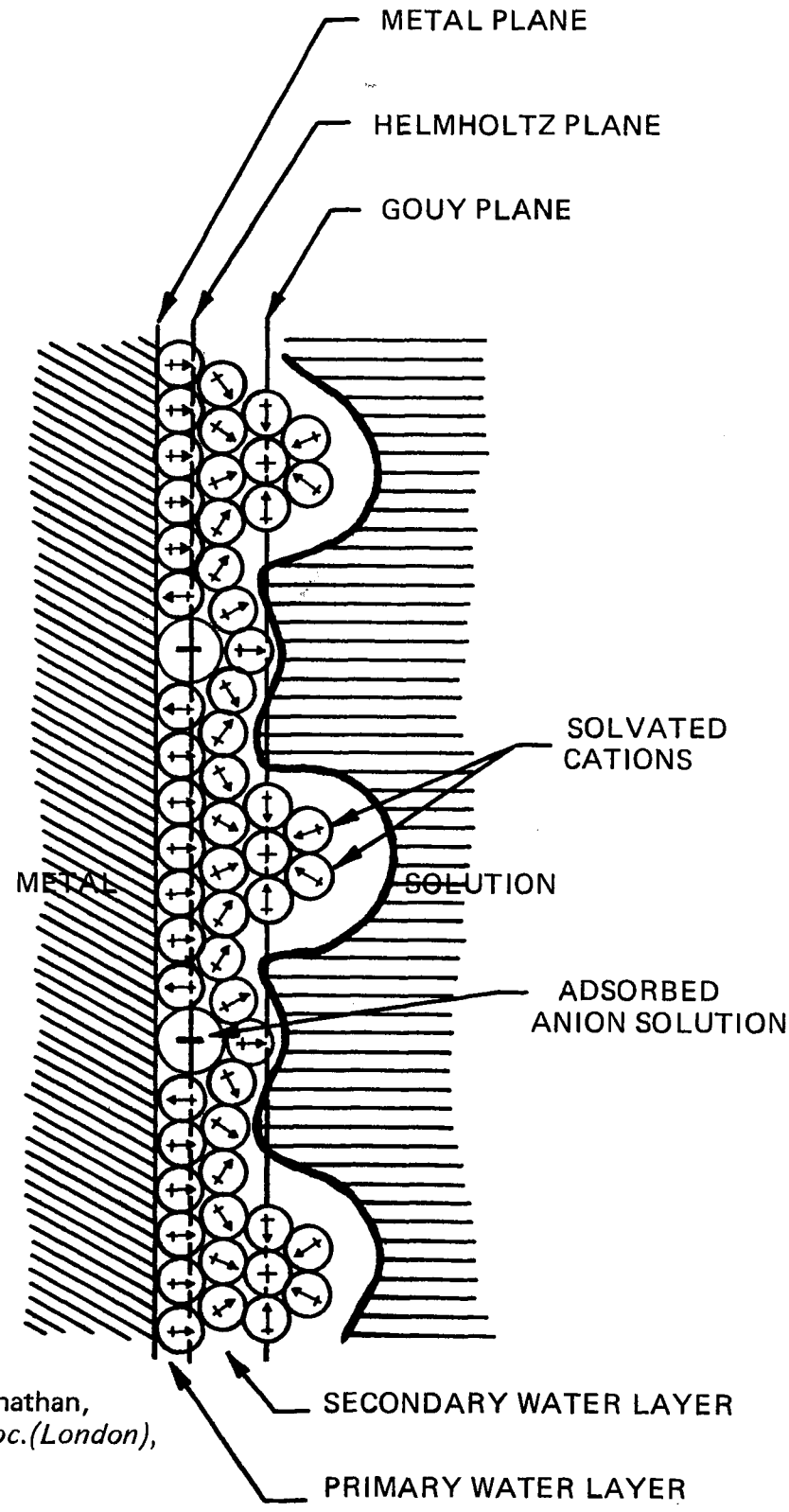

J. O'M. Bockris, M. A. Devanathan, and K. Müller, *Proc. Roy. Soc.(London)*, A274, 55 (1963).

It would be suspected that the largest grains form at the longest ON times since this situation produces the largest and fewest nucleation sites. The smallest grains form at the lowest duty cycles since this situation produces the highest adion concentration and, as a result, the highest number of nucleation sites. This model agrees with the experimentally observed pattern of grain growth dependence on pulse waveform for limited cases, which will be clarified in the next section. The short duty cycles are experimentally found to have the finest grain structure. The dependence of grain size on ON time duration is only observed at long duty cycles $>$ 50%. At duty cycles $<$ 50%, another factor, the crystallographic orientation enters the model of grain growth. This aspect is considered in the following section.

V. Preferred Orientation

A. Introduction

A polycrystalline metal exhibits preferred orientation when a particular crystallographic plane predominates in the direction parallel to the substrate. In a thin film, a (h,k,l) preferred orientation denotes the planes in which Miller indices h, k, l tend to be parallel to the film surface. Thin metal films have previously been characterized by x-ray diffraction when deposited by methods other than pulse plating. Studies of gold films deposited in vacuum by evaporation showed a strong (111) orientation which upon annealing tended toward (200) orientation and accompanying grain growth.[40] The orientation of structure implies a directional dependence of the mechanical properties of the gold film[41]. In electronic applications where mechanical properties are significant, such as in thermocompression bonding, preferred orientation may be as important as microstructure in governing the character of the deposit.

B. Objective

X-ray diffraction was performed on the same specimens which were examined by scanning electron microscopy. The purpose was to determine preferences in atomic orientation which are promoted by waveform variations.

C. Experimental

The method of McClintock[42] was used to relate diffraction pattern features to the crystallographic orientation of the diffracting grains. Using the specimen orientation and the geometry of the wide-film cylindrical camera, McClintock derived the relationship:

$$\cos W_{hkl} = \cos \psi \quad \cos \theta_{hkl} \quad \cos \zeta \; + \; \sin \psi \quad \sin \theta_{hkl}$$

where W_{hkl} is the angle between the reflecting hkl plane and the plane having preferred orientation, i.e. parallel to the specimen surface ψ, is the camera angle, the angle between the incident x-ray beam and the specimen surface, θ_{hkl}, is the Bragg angle of the hkl plane,

and ψ is the angle made by an individual intensity peak on the developed negative, measured by superimposing the negative on a grid provided by McClintock. Values of W_{hkl} are calculated from ψ, the θ_{hkl} of each hkl diffraction line and the ζ's of the individual intensity peaks along the lines. The W_{hkl}'s are then compared to the interplanar angles tabulated by Cullity.[43] The planes tending to be parallel to the surface are noted giving the preferred orientation.

D. Results of Diffraction Patterns

The preferred orientation relations showed during the study may be summarized with respect to two aspects of the waveform variation: first, ON time variation, i.e. the orientation change in deposits formed at the same duty cycles but different ON times; second, OFF time variation, i.e. deposits formed at the same ON time but at different duty cycles.

1. Effect of ON Time

a. At the 9% duty cycle (111) orientation is found at 0.1 msec ON. At longer ON times (111)-(200) orientation is apparent. The (111) orientation was predeminantly parallel to the specimen surface and the (200) at approximately a 14° to 19° angle to the surface. At the short ON times (0.3, 0.5, 0.7, 1.0 millisecond ON) the (111) predominates and (200) is muted. As the ON time increases (2.0, 2.4, 6.0, 8.0, 9.0 milliseconds) the (200) orientation becomes stronger.

b. The one sample at 25% duty cycle with 1.0 msec ON: 3.0 msec OFF had only slight (111) orientation and no (200), approaching a random orientation.

c. The 33% duty cycle was predominantly (111) at short ON times (i.e. 0.5 msec ON) with only traces of (200). At ON times greater than 2 msec, (200) orientation became pronounced and dual orientation, (111) and (200) was apparent.

d. The 50% duty cycle is (111) at short ON time (1-2 msec ON) with randomness apparent at 4 msec ON. With increasing ON time (6 msec) the (111) orientation strengthens and (200) is present. At the longest ON times, strong dual orientation is apparent.

e. The limited samples at 66%, 75%, and 90% duty cycles were predominantly (111) with only traces of (200) orientation.

2. Effect of OFF Time (i.e. Duty Cycle)

Six sets of samples having the same ON time but different OFF times were compared:

a. 0.5 msec ON

Duty Cycle	OFF Time	Preferred Orientation
9%	5 msec	Strong Dual (111)-(200)
33%	1 msec	(111), trace of (200)

b. 1 msec ON

Duty Cycle	OFF Time	Preferred Orientation
9%	10 msec	Strong Dual (111)-(200)
25%	3 msec	Some (111), largely random
33%	2 msec	(111), trace of (200)
50%	1 msec	(111), trace of (200)

c. 2 msec ON Time

Duty Cycle	OFF Time	Preferred Orientation
9%	20 msec	Strong Dual (111)-(200)
33%	4 msec	Dual (111)-(200)
50%	2 msec	Slight (111), trace of (200)
66%	1 msec	Slight (111), trace of (200)

d. 4 msec ON Time

Duty Cycle	OFF Time	Preferred Orientation
9%	40 msec	Dual (111)-(200)
33%	8 msec	Dual (111)-(200)
50%	4 msec	Slight (111) almost random
66%	2 msec	Slight (111) almost random

e. 6 msec ON Time

Duty Cycle	OFF Time	Preferred Orientation
9%	60 msec	Dual (111)-(200)
33%	12 msec	Dual (111)-(200)
50%	6 msec	Predominantly (111); (200) apparent
75%	2 msec	Slight (111) approaching random

f. 8 msec ON Time

Duty Cycle	OFF Time	Preferred Orientation
9%	80 msec	Dual (111)-(200)
50%	8 msec	Dual (111)-(200)
66%	4 msec	Slight (111)

E. Discussion

At short duty cycles (e.g. 9%), there is the least change in orientation with ON time. The orientation is dual (111)-(200) in these deposits at ON times of 3 msec or greater. The (200) orientation strengthens with increasing ON time and decreasing duty cycle. The changes in orientation at higher duty cycles is more pronounced. At duty cycles of 33% and better there is an apparent shift from predominantly (111), through a random orientation to a dual (111) (200) orientation as the ON time increases. The longest duty cycles, 75% and 90%, exhibit random and (111) orientation.

These changes in orientation parallel the shifts in grain size discussed in the previous section concerning microstructure. Reconsidering the formula for rate of nucleation:

$$R = 2\pi r_c n^2 \left(\frac{kT}{2\pi m}\right)^{1/2} \quad \exp\left[-\frac{\Delta F_c + E}{kT}\right]$$

Where r_c = critical radius of the nucleus

n = no. of adions/cm^2

ΔF_c = free energy for formation of the nucleus

E = activation energy for surface diffusion

At low impingement rates where the number of adions/cm^2, n, is small, the (111) orientation is favored since this orientation has the lowest activation energy for surface diffusion, E. Three atoms connected in a triangle in the same plane (Figures 43-1,2,3a) result in the (111) orientation parallel to the surface. There are two bonds/atom in this nucleus and as a result it has a less favorable free energy formation, ΔF_c, than the (200) orientation which has 3 or 4 bonds/atom in the nucleus.

The nucleus with the (200) orientation is the square based pyramid (Figures 43-3b) with the top atom having four bonds and the base plane atoms having three bonds. The activation energy for diffusion, E, is greater for the (200) orientation since an adion must leave the surface plane and diffuse to the top position on the pyramid or, less likely, must diffuse directly from solution to the pyramid top.

At high impingement rates e.g. short duty cycles, it is found experimentally that the (200) orientation is formed. With decreasing duty cycle the instantaneous concentration of adions available for deposition increases. The collision theory of reaction rates predicts that attaining an activation energy, E, becomes increasingly probable as the concentration per volume per time increases. It is reasonable to propose that at short duty cycles, high adion concentrations aid in surmounting the activation energy barrier and the (200) orienta-

FIG. 43: ATOMIC ORIENTATION IN NUCLEI

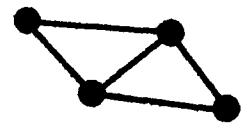

1. INITIAL CLUSTER OF 4 PLANAR ATOMS

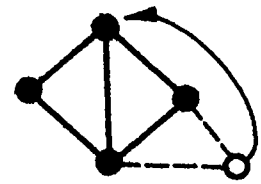

2. DIFFUSION OF AN ADDITIONAL ATOM TO THE CLUSTER

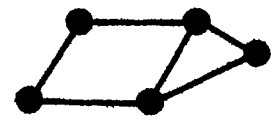

3a. ADDITIONAL ATOM ATTACHES IN (111) ORIENTATION

OR

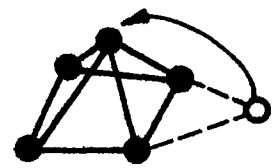

3b. ADDITIONAL ATOM ATTACHES IN (200) ORIENTATION

tion, which has a more favorable free energy of formation than the (111) orientation, is formed.

Extension of this model suggests an explanation for the observed pattern of grain size which compliments the adion considerations previously discussed. Consider a quantity, P, the degree of preferred (200) orientation, which may be defined as:

$$P = \frac{N_{200}}{N_T} + 1$$

where N_{200} is the number of grains with (200) orientation/unit area and N_T is the total number of grains/unit area.

The free energy of formation for a critical nucleus, ΔF_c, ($\Delta F_c < 0$) becomes more negative with increasing (200) orientation. This results from the increased binding energy in the (200) orientation i.e. 3 or 4 bonds/atom in the nucleus, compared to the (111) orientation i.e. 2 bonds/atom in the nucleus. Thus:

$$-\Delta F_c \propto P$$

For nucleation to be thermodynamically favorable the free energy of formation, ΔF_c, must outweigh the energy of activation for surface diffusion, E. Since (200) orientation is experimentally observed:

$$\Delta F_c + E < 0$$

Consider the nucleation rate equation previously described:

$$R = 2\pi r_c n^2 \left(\frac{kT}{2\pi m}\right)^{1/2} \exp\left[-\frac{\Delta F_c + E}{kT}\right]$$

$$R \propto \exp\left[-\frac{\Delta F_c + E}{kT}\right]$$

Since $-\Delta F_c \propto P$, then as P increases, $-\frac{\Delta F_c + E}{kT}$ increases:

$$P \propto -\frac{\Delta F_c + E}{kT}$$

Therefore:

$$R \propto \exp^{P}$$

Increasing (200) orientation thus increases the nucleation rate.

The (200) orientation increases with ON time and decreases with duty cycle.

$$P \propto \text{ON time}$$

$$P \propto \frac{1}{\text{Duty Cycle}}$$

Experimentally, a decrease in grain size with increase in ON time is least noticeable at the shortest duty cycle. This is because strong dual orientation is constant at the 9% duty cycle above 0.1 msec ON. However, the shift to dual orientation (111)-(200) occurs at 4 to 6 msec ON for the 50% duty cycle and 1-2 msec ON for the 33% duty cycle and 0.1-0.3 msec ON for the 9% duty cycle. In these cases the grain size decreases with ON time as the orientation shifts.

$$\text{Grain Size} \propto \frac{1}{R}$$

$$\text{Grain Size} \propto \frac{1}{\exp^{\text{ON time}}}$$

Similarly grain size should increase with duty cycle.

$$\text{Grain Size} \propto \exp^{\text{Duty Cycle}}$$

This model compliments the effects of adion concentration, on grain size which were discussed in the previous section on microstructure. The exponential factor provides a conceptual description of the grain size variations that occur at long ON times and at duty cycles less than 66% where shifts in orientation occur.

VI. Internal Stress

A. Introduction

Stresses created during electrodeposition have been suspected sources of adhesion failures and open circuits in thin film circuits.

The orientation shift from (111) to dual (111)-(200) found in the short duty cycle pulse-plated films is similar to reported[40] shifts occuring during the annealing of evaporated gold films. This analogy suggested that a comparison of the stresses in the pulse plated gold, which had a dual orientation, with those in D.C. plated gold, which is (111), would be of interest. Measurements of the net internal stresses were made using the Brenner Senderhoff technique for the purpose of discerning stress differences between pulse gold with (111)-(200) orientation and D.C. plated gold with (111). The pulse plating was as the 90% duty cycle with 0.9 msec ON: 9.0 msec OFF.

B. Experimental Method of Brenner and Senderhoff

A contractometer (Figure 44) of the design proposed by Brenner and Senderhoff[45] was used to measure the net internal stress in plated gold films. This apparatus simply consists of a copper or copper-clad helix and a gauge for recording the deformation of the helix. The helix is calibrated initially by measuring the deformation resulting from the application of a known stress. The helix is plated following calibration. The stress created during plating is determined from the measured helix deformation. The basic relation for this calculation is:

$$S_t = \frac{Et^2\, p^D}{1.08 \times 10^4\, Chd} \left(\frac{1 + Eod}{Et} \right)$$

FIG. 44: BRENNER-SENDERHOFF CONTRACTOMETER

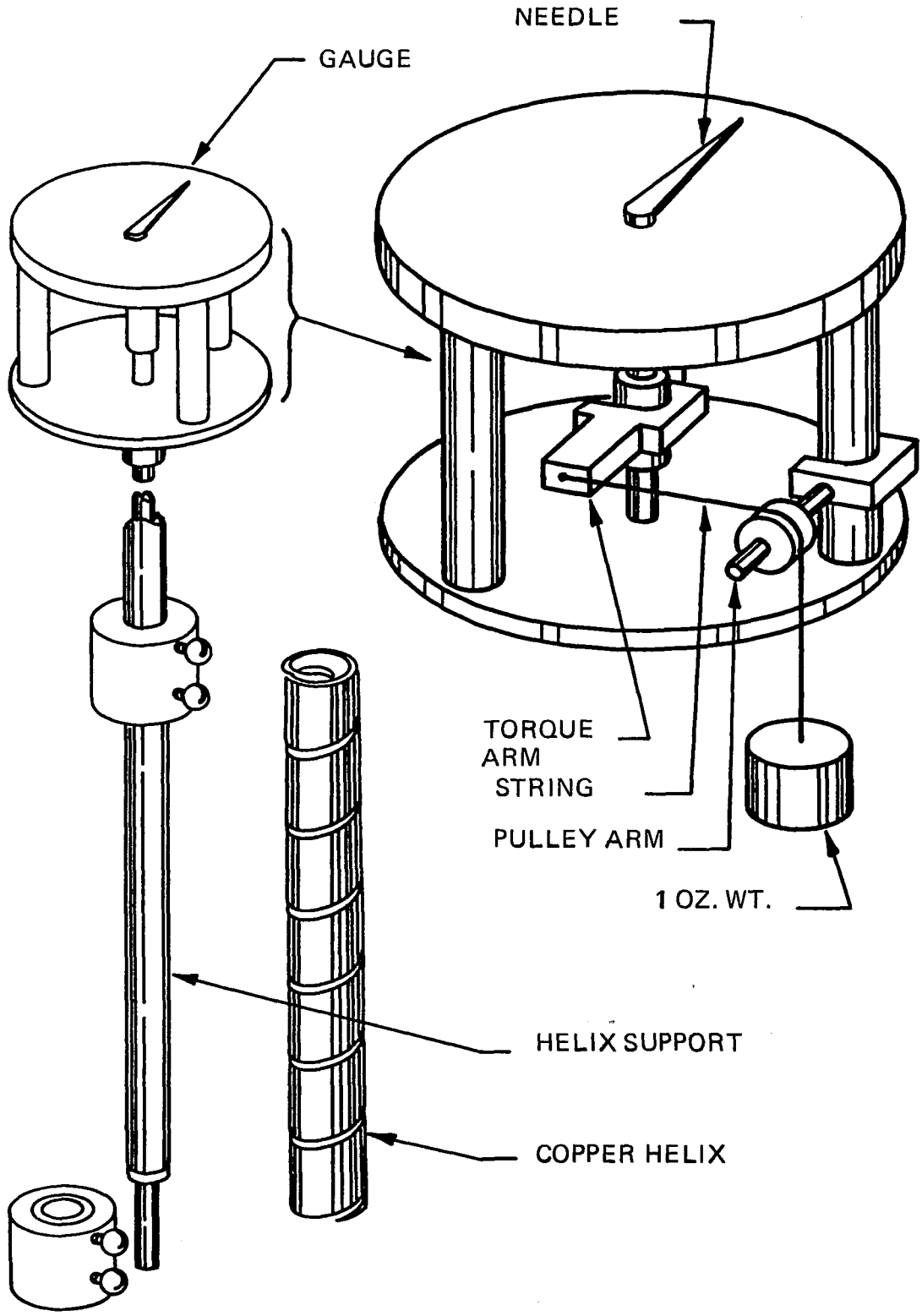

where S_t = stress

C = diameter of helix

d = thickness of deposit

D = gauge deflection

Eo = Young's modulus of film

E = Young's modulus of helix

h = height of helix plated

t = thickness of helix

p = pitch of helix

C. Results See Figure 45 and Tables 3-4

D. Discussion

The stress measured by the Brenner-Senderhoff contractometer is the net stress of the gold film. There are three principle stress contributions which compose the new measurement. One factor, the interfacial stress, is particularly sensitive to substrate effects. Experimental design required the deposition of gold to be on a copper helix. The following sections review the general mechanisms related to the presence of internal stresses as abstracted from the literature.

1. Interfacial Stress [46,47,48]

The Van der Merwe theory describes the structural conditions of an interface in relation to the lattice mismatch occurring at the interface of materials with similar structures. For example, copper and gold have similar crystal structures; they are face centered cubic metal with lattice constants of 3.6150A, and 4.0786A respectively. Consideration of the growth of a single crystallite of gold on a crystallite of copper in their polycrystalline matrices, leads to the following model. Initially, there is a growth of discrete epitaxial films on the substrate grains forming an immobile monolayer. This film is homogeneously deformed to fit the lattice spacing of the substrate

FIG. 45: STRESS vs. THICKNESS

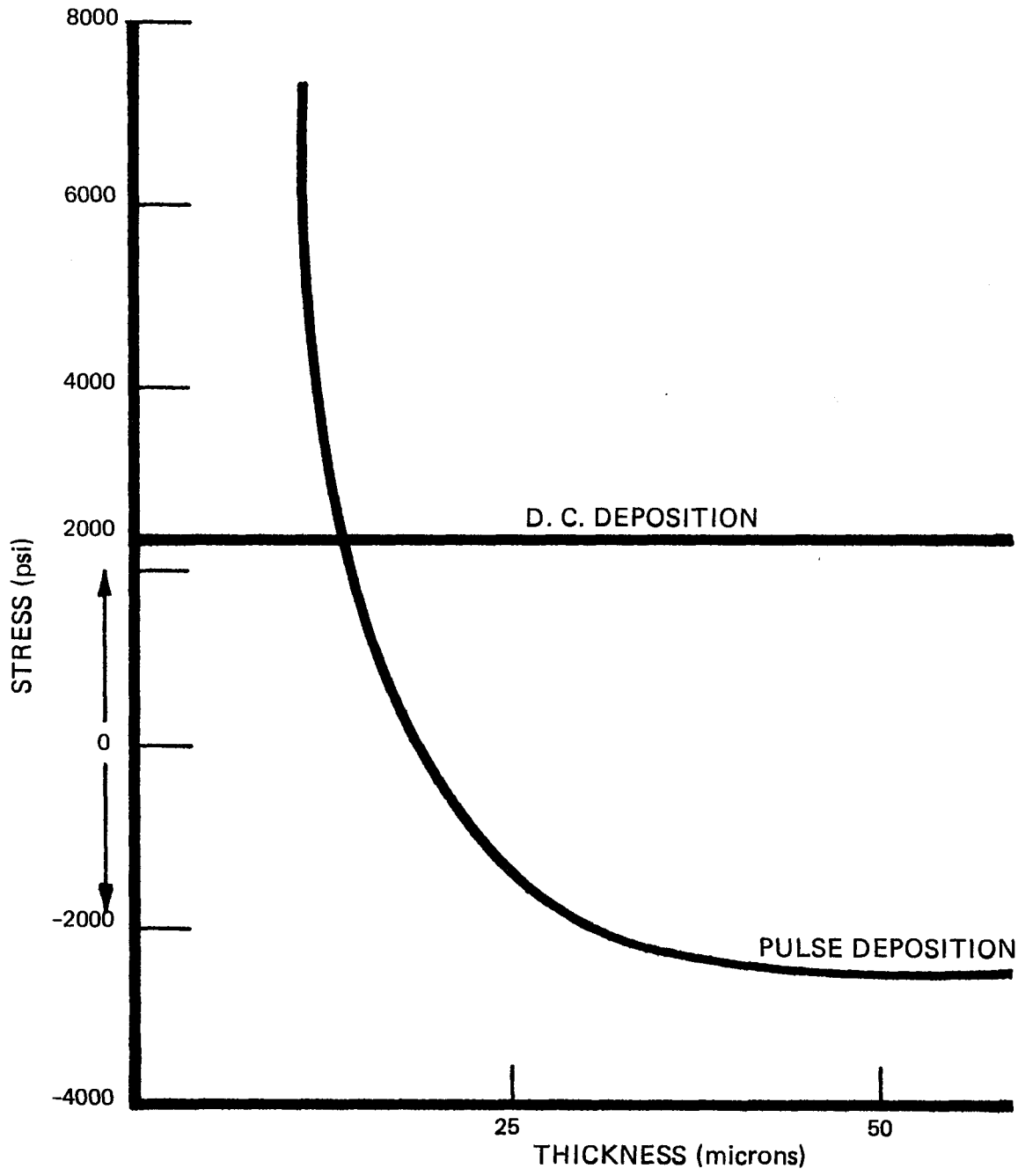

TABLE 3: D. C. PLATED GOLD FILMS

SAMPLE NO.	THICKNESS	STRESS	TYPE
1	7.31μ	2481 psi	Tensile
2	9.95μ	2017 psi	Tensile
3	14.73μ	2391 psi	Tensile
4	16.03μ	2246 psi	Tensile
5	22.86μ	2220 psi	Tensile
6	26.16μ	2244 psi	Tensile

Mean Stress = 2266 psi
Standard Error of Mean Stress = 65 psi
Standard Deviation = 159 psi

TABLE 4: PULSE PLATED GOLD FILMS

SAMPLE NO.	THICKNESS	STRESS	TYPE
1	10.19μ	6397 psi	Tensile
2	10.31μ	3163 psi	Tensile
3	12.78μ	7306 psi	Tensile
4	27.43μ	-1735 psi	Compressive
5	30.48μ	-2000 psi	Compressive
6	47.50μ	-2432 psi	Compressive
7	57.66μ	-2297 psi	Compresive

Average Current Density, 4 amp/ft.^{2}

layer. Experimental evidence has verified that this model is applicable to film systems with misfits less than 14%. Misfit is defined mathematically by the following form:

$$\text{Misfit} = f = \frac{(b-a)}{1/2\ (a+b)}$$

where a = lattice constant of substrate material

b = lattice constant of deposited material

For gold on copper the calculated misfit is 12.05%. As a result of this misfit, an array of parallel edge dislocations are formed to accommodate the difference in lattice spacing.

The compressive stress decreases as the thickness of the crystallite increases. The edge dislocations alleviate the interfacial strain and the lattice spacings of gold atoms tend to that of bulk gold as they are deposited more distantly from the interface. Interfacial dislocations can grow to line dislocations which surface on grain boundaries. Repulsion of similar dislocations accentuates this process. The less the thickness at which nuclei coalesce, the less the stress relief in the continuous film. Stress relief by surfacing dislocations is inhibited by the grain junction. The smaller the grain the higher is the interfacial stress contribution. Pulse plated films, which are fine grained, should thus have a high interfacial stress contribution.

2. Volume Contraction and Expansion[50]

Condensation of impurities and the formation of condensed vacancy clusters on dislocations inhibits dislocation migration to grain surfaces. When migration is sufficiently retarded, withdrawal of dislocations to the surface will cease. When this state is reached a stressed condition occurs. The interfacial grain layer may contain up to 5% voids.[51] The subsequent layers have lattice spacing similar to bulk gold and, thus, have a reduced lattice spacing. This reduction is opposed by the interfacial

adhesion creating a tensile stress condition. The effect can be enhanced by the coalescence of crystallites, further reducing the volume. Volume expansion resulting from shifts in orientation would produce an opposite stress condition.

3. Sorption Contribution to Stress [50,51]

The operation of adsorption mechanism counteracts volume contraction. There is a tendency toward expansion created by the adsorption of slight amounts of foreign impurities in the deposit. The expansion contributes a compressive stress factor to the deposit. As adsorption occurs, impurities are "overgrown" by neighboring crystals. Charged foreign substances or those with induced or permanent dipole moments can be readily adsorbed under the influence of the electric field present during deposition. Additives, ions of electrolyte, dipole molecules of water, etc. are all candidates for adsorption. When these impurities are present deep in the deposit, without electric field restriction of thermal movement, the thermal motion they exert is sufficient to create plastic deformation of grains.

Thus, in plated gold films, there are generally three primary factors contributing to stress: (1) interfacial mismatch, (2) volume contraction and expansion, and (3) impurity sorption.

Evaporated gold deposits are governed by the same considerations as those discussed for electrodeposited gold. In addition, a most significant contribution to tensile stress in evaporated materials is the contraction of upper regions of the growing deposit as they cool after deposition.[50] The thermal contraction is analogous to the volume contraction factor of plated films. A number of other mechanisms, all tensile, have been reported for evaporated films.[52] These can be considered as analogous to the contraction model. It would be expected from the predominance of tensile contribution that evaporated films would be more highly tensile in character than plated

counterparts. Values reported for tensile stress of evaporated gold range from 30,000 to 40,000 psi,[53] significantly higher than stress values obtained on plated films.

The samples examined that were prepared by D.C. plating consistently gave tensile values slightly greater than 2000 psi, a mean of 2266 psi. Direct variation of stress with thickness in the 8μ to 25μ range was not observed.

Stress values obtained for pulse plated films range from tensile to compressive, and a definite dependence on thickness is observed. At thicknesses of a 25μ or less, tensile stresses were observed. Grain size in the pulse plated gold is finer than in the D.C. plated film. Both tensile and compressive stress factors are reportedly[51] inversely proportional to the square root of the mean grain size.

$\sigma \propto a^{1/2}$

σ = stress

a = mean grain size

A film with fine grain structure is more sensitive to variations in factors contributing to stress than films with large grains. Pulse plated films of thicknesses greater than 25μ produced compressive stresses. A higher field potential is needed in pulse plating than in D.C. plating to drive the peak current pulse. Dipoles and extraneous impurities can be driven into the lattice structure as a result of the high field potential. This could produce a significant sorption contribution. Volume expansion and sorption expansion are both mechanisms which could produce the compressive stress observed experimentally in thick pulse plated films.

VII. Throwing Efficiency

A. Introduction

In a preceding section the dependence of thickness distribution on waveform was investigated for planar deposits. Thickness distribution for deposits which are not planar, but are irregular, can be quantitatively measured in terms of throwing efficiency.

The throwing efficiency was obtained for each of the pulse waveforms listed in Table 1 using the method developed by Haring and Blum.[55] The object was to determine what effect the nature of the pulse waveform would have on the metal distribution when deposition occurs on irregular substrates.

B. Procedure

A Haring cell is a rectangular plating tank containing positions for an anode and two cathodes (i.e. sample substrates, in this case, brass Hull cell panels) arranged parallel (Figure 46). This arrangement places a uniform electric field on the cathodic substrates when they are electrically connected. The perforated anode is positioned so that the distance from the one sample is five times greater than the distance from the other. This gives a primary current density ratio , K, between the two cathodes of 5 to 1. The weight of each sample cathode is recorded before and after deposition. The ratio of the weight gains gives the metal distribution ratio, M. According to the suggestion of Pan[56] the throwing efficiency was calculated from the following relationship:

$$\text{Throwing Efficiency} = \frac{100\,(K-M)}{K-1}$$

From this relationship the ideal, perfect throwing power would have an efficiency of 100%.

Data treatments other than throwing efficiency can be used to describe the primary current distribution. This distribution is often referred to in terms of macrothrowing power. Other methods of describing throwing ability will be discussed in the section on cathode efficiency where their numerical values are amenable to being plotted on the same

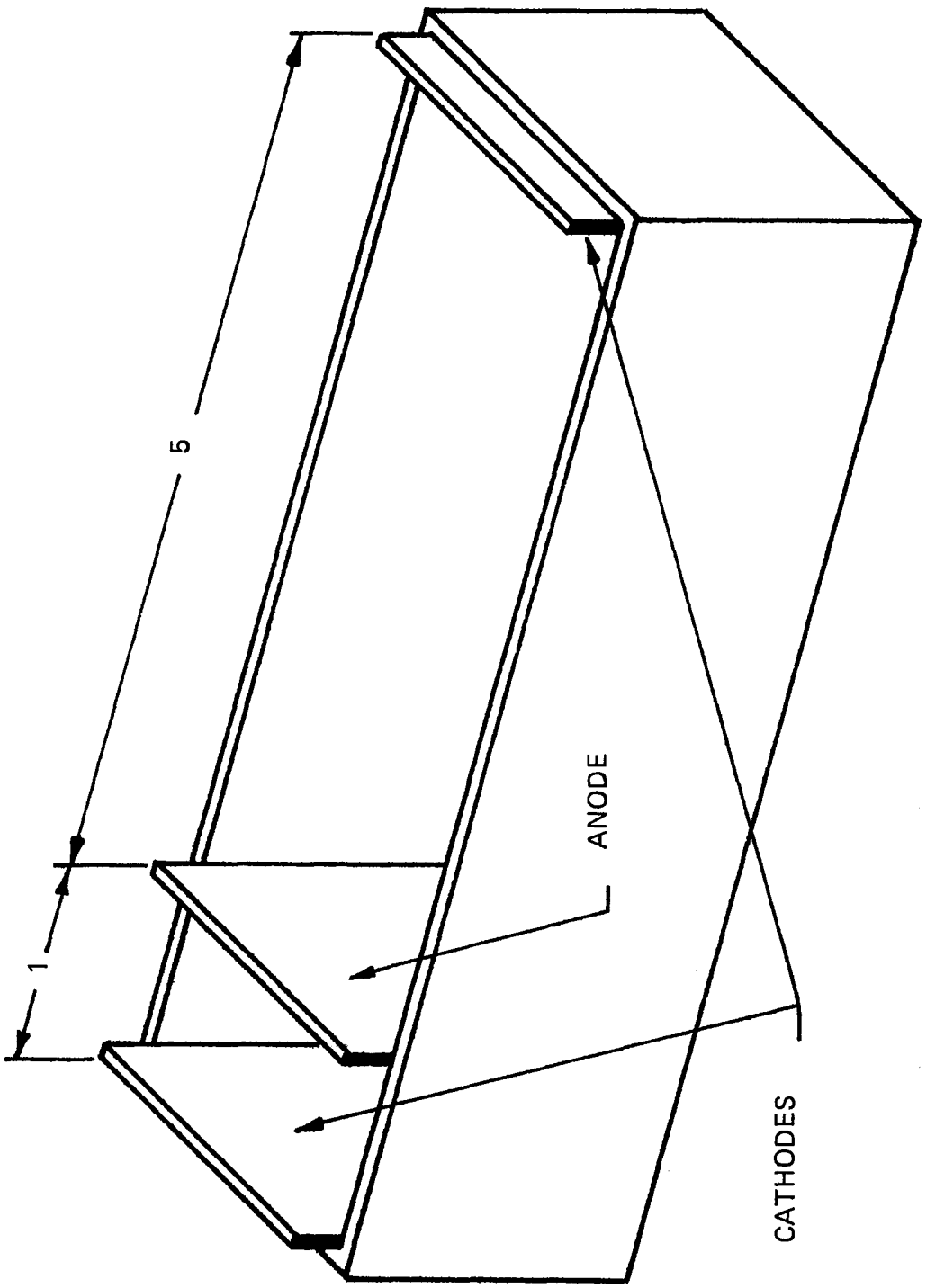

FIG. 46: HARING CELL

graph as cathode efficiency. Qualitatively, these data treatments are similar to throwing efficiency.

C. Discussion

The calculated values of throwing efficiency are listed in Table 5 and plotted against log ON time in Figure 47.

At duty cycles less than 50%, a similar pattern in throwing efficiency among duty cycles exists. With the exception of the outlying point at 0.1 msec ON for 9%, there is an upward trend in efficiency with ON time reaching a maximum at 1 msec ON. At ON times greater than 1 msec throwing efficiency tends to decrease.

The exceptions to this trend were samples deposited at long ON times and high duty cycles. The duty cycles of 75% and 90% with 9 msec ON both had high throwing efficiency of 94%, and 99% respectively. D.C. deposition had an efficiency of 91%. The same increase in macrothrowing power has been found for long cycles with periodic reverse current in copper deposition.[57]

TABLE 5: HARING CELL RESULTS

NO.	DUTY CYCLE %	ON–OFF TIME	%CATHODE EFFICIENCY	%THROWING* EFFICIENCY	%THROWING** POWER	%THROWING*** POWER
1	9	0.1-1	78.2	94.8	75.9	78.6
2	9	0.3-3	64.8	84.8	67.9	52.8
3	9	0.5-5	57.3	86.0	68.8	55.1
4	9	0.7-7	76.3	92.1	73.7	70.0
5	9	1.0-10	76.2	94.5	75.6	77.5
6	9	2.0-20	69.2	93.1	74.5	72.9
7	9	4.0-40	68.3	86.6	69.3	56.5
8	9	6.0-60	57.4	86.7	68.0	53.0
9	9	8.0-80	58.0	76.3	61.0	39.2
10	9	9.0-90	71.9	78.3	62.7	42.0
11	33	0.5-1	72.2	94.0	75.2	77.8
12	33	1.0-2	70.8	92.6	74.1	71.4
13	33	2.0-4	70.0	92.4	73.9	70.8
14	33	4.0-8	71.4	90.3	72.3	65.1
15	33	6.0-12	61.5	83.7	66.9	50.6
16	33	8.0-16	66.3	81.7	65.4	47.3
17	33	9.0-18	14.3	83.0	66.4	49.4
18	50	1.0-1	59.3	82.5	66.0	48.4

NO.	DUTY CYCLE %	ON–OFF TIME	%CATHODE EFFICIENCY	%THROWING* EFFICIENCY	%THROWING** POWER	%THROWING*** POWER
19	50	2.0-2	59.0	85.3	68.2	53.7
20	50	4.0-4	61.8	85.8	68.6	54.8
21	50	6.0-6	60.5	84.6	67.6	52.2
22	50	8.0-8	60.9	82.3	65.8	48.2
23	50	9.0-9	61.2	82.8	66.3	49.1
24	66	2.0-1	57.3	76.6	61.3	39.6
25	66	4.0-2	51.9	73.3	58.6	35.4
26	66	8.0-4	54.9	75.8	60.6	38.5
27	75	6.0-2	48.5	82.9	66.3	49.2
28	75	9.0-3	29.5	93.7	74.9	74.8
29	90	9.0-1	38.5	99.0	79.2	95.3
30	2.5	1.0-3	56.9	84.6	67.2	52.4
31	D.C.		63.6	90.9	72.7	66.6

* After Pan $\frac{100(K-M)}{K-1}$

** After Fields $\frac{100(K-M)}{K}$

*** After Subramanian $\frac{100(K-M)}{M(K-1)}$

FIG. 47: THROWING EFFICIENCY vs. LOG ON TIME

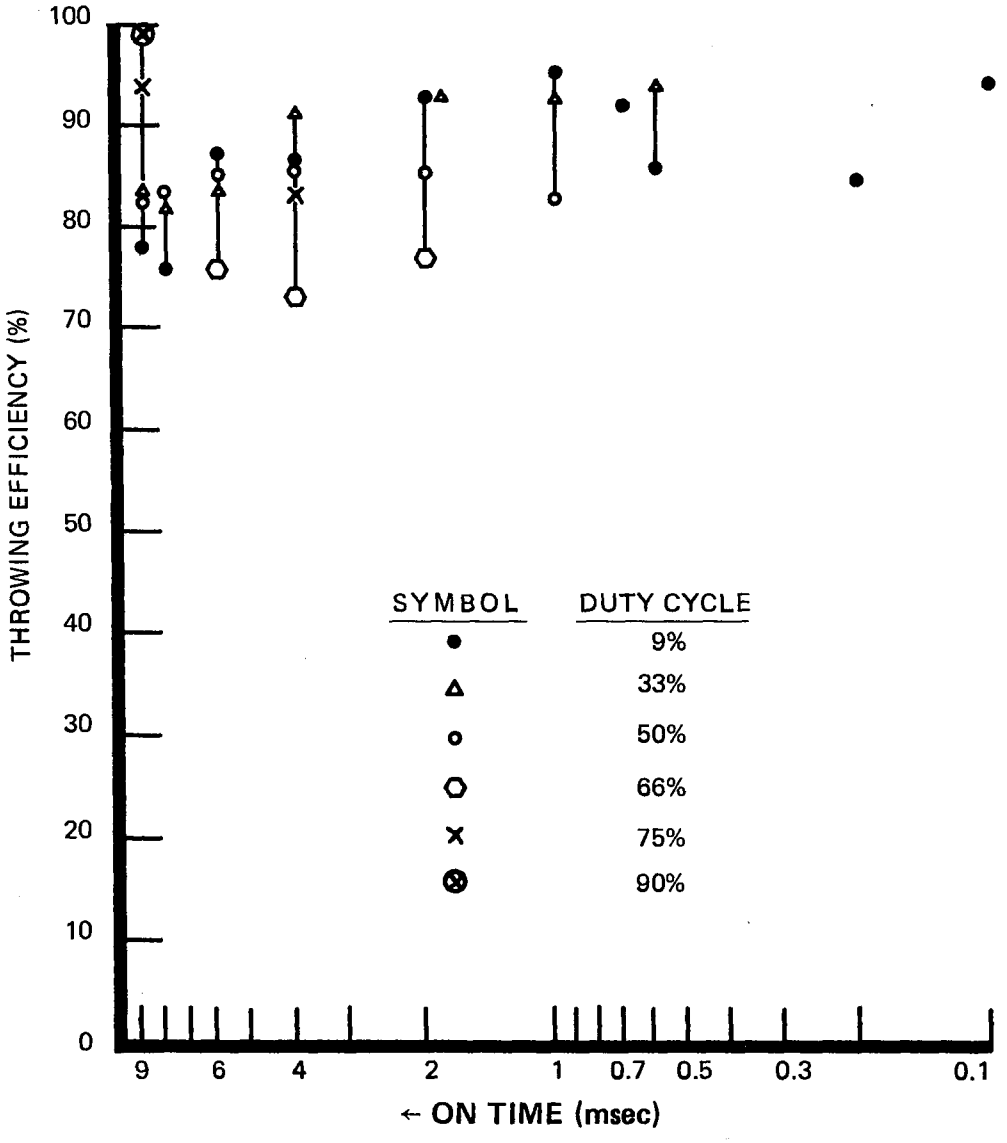

VIII. Cathode Efficiency

A. Introduction

The cathode efficiency is a measure of the current actually utilized in deposition compared to the theoretical maximum current available for deposition. The difference is indicative of the amount of the current involved with side reactions. The objective in determining cathode efficiencies was to determine the affect pulse-waveform variations produced on the deposition reaction.

B. Calculation From Faraday's Laws

The cathode efficiencies were calculated for samples deposited at each of the waveform conditions in Table 1. One sample set was at constant agitation, another was deposited without agitation. This latter set was deposited in the Haring Cell for measuring macrothrowing power.

The actual current contributing to deposition is measured by the weight gain of the sample. The theoretical weight deposited is calculated according to Faraday's laws:
1. The quantity of an element discharged at an electrode is proportional to the quantity of electricity that is passed. 2. The quantities of different elements discharged by a given quantity of electricity are proportional to the electrochemical equivalents of those elements. For the gold system being considered the equivalent weight per ampere-minute is 122.7 mg. The theoretical weight to be deposited is then:

$$\underset{(mg)}{\text{Theoretical Wt.}} = \underset{(amp)}{\text{Peak Current}} \times \underset{(min)}{\text{Time}} \times \text{Duty Cycle} \times \underset{(mg/amp.min)}{122.7}$$

The cathode efficiency is:

$$\text{Cathode Efficiency} = \frac{\text{Wt. Gain}}{\text{Theoretical Wt.}}$$

C. Discussion

The results are plotted in Figure 48 asCathodeEfficiency versus log ON time for the set of samples with high agitation. There is a decrease in efficiency with increased ON time. The most drastic reduction in efficiency occurs with 9 msec ON. This is attributable to the local depletion of metal ion species available for deposition at the cathode during peak current flow for long ON times. The result is hydrogen evolution from water electrolysis and drastic reduction in cathode efficiency.

The cathode efficiencies of the samples deposited in the Haring Cell, without agitation, are plotted in Figures 49-52. As in the case of the samples deposited with agitation, the cathode efficiency decreases with increasing ON time. The lack of agitation increased side reactions at shorter ON times as well. The efficiencies for the samples were 20 to 40% lower than at the same deposition conditions with agitation. The deposits formed by D.C. current at low agitation had a cathode efficiency of 63% and a throwing power of 72%.

Throwing power is a concept similar to throwing efficiency. The definition which was used for the calculations is the one provided by Subramanian.[54]

$$\text{Throwing Power} = \frac{100\ (K-M)}{M\ (K-L)}$$

This concept is used in this section simply because it provides a wider spread in numerical values that can be plotted clearly on the same coordinates as cathode efficiency. Basically, it is the same as throwing efficiency in its qualitative description.

Plots of throwing power versus log ON time were made along with plots of cathode efficiency versus log ON time on the same sets of coordinates. A plot at the 9% duty cycle is shown in Figure49,33% duty cycle in Figure 50 , 50% duty cycle in Figure 51 and 66%, 75%, and 90% in Figure 52. The plots illustrate that the throwing power closely follows cathode efficiency. The exception is the 9 msec ON time with 75% and 90% duty cycles. In these cases throwing power increases notably while cathode efficiency drops and hydrogen

FIG. 48: CATHODE EFFICIENCY vs. LOG ON TIME

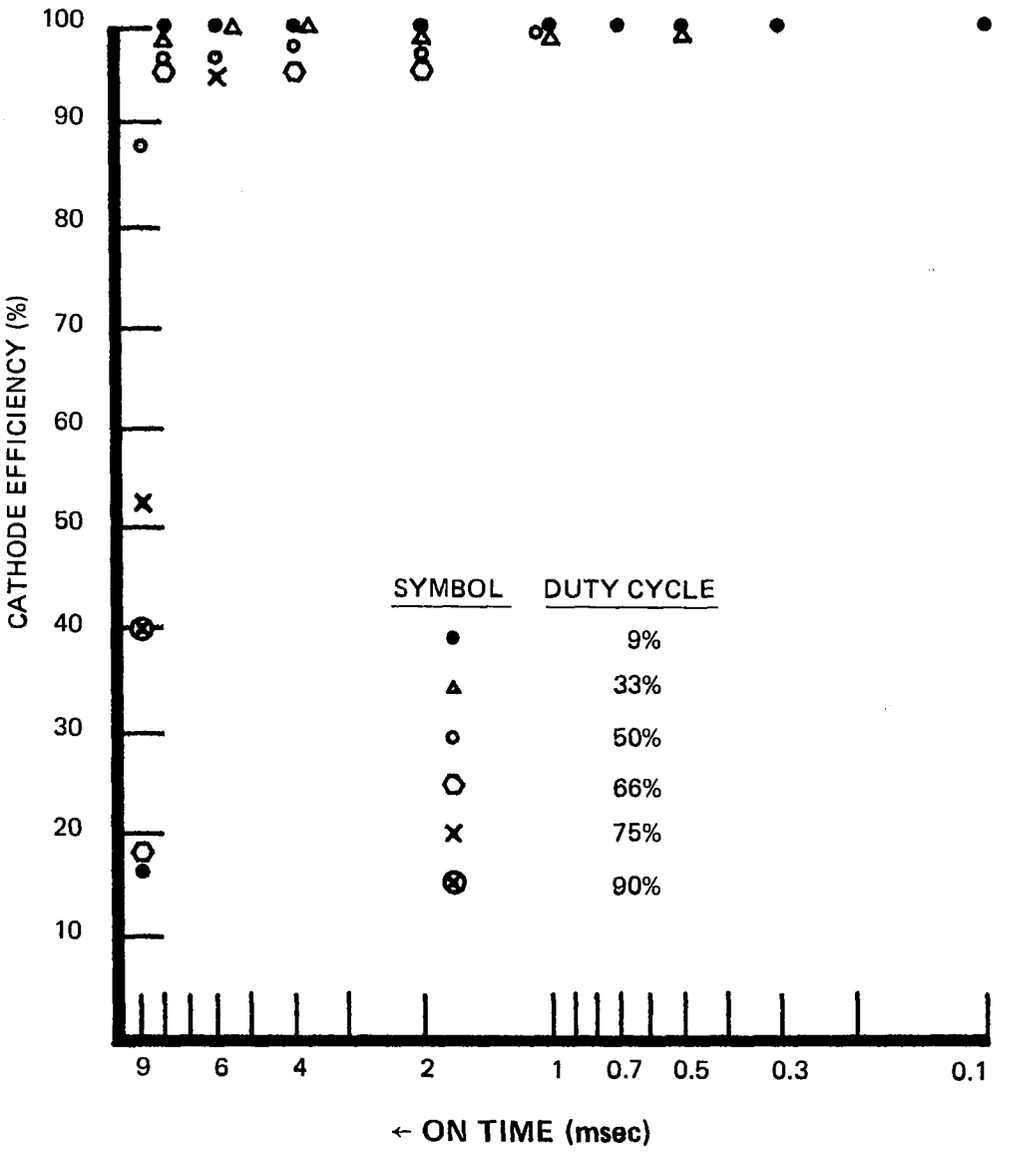

FIG. 49: THROWING POWER vs. LOG ON TIME AND CATHODE EFFICIENCY vs. LOG ON TIME FOR 9% DUTY CYCLE

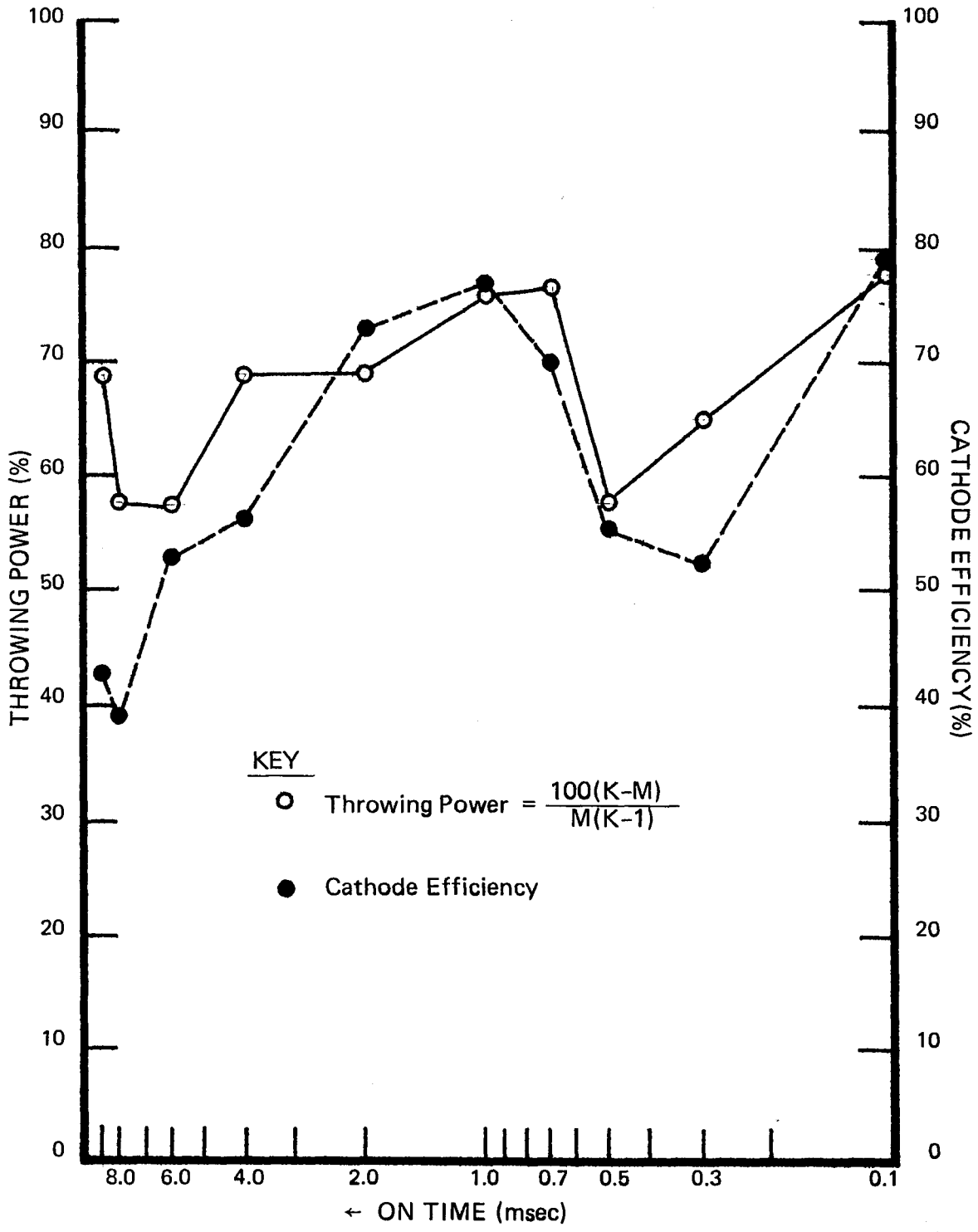

FIG. 50: THROWING POWER vs. LOG ON TIME AND CATHODE EFFICIENCY vs. LOG ON TIME FOR 33% DUTY CYCLE

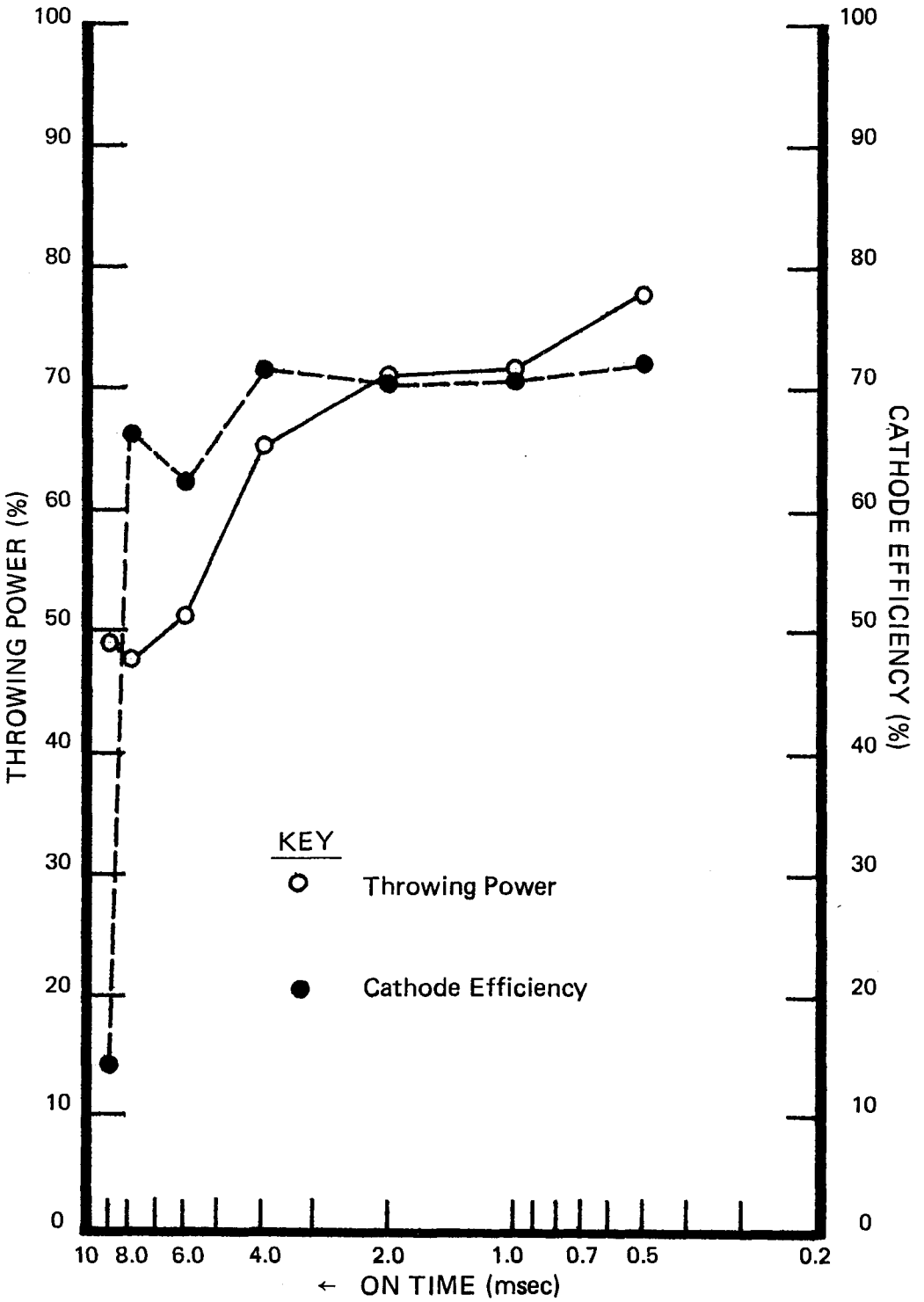

FIG. 51: THROWING POWER vs. LOG ON TIME AND CATHODE EFFICIENCY vs. LOG ON TIME FOR 50% DUTY CYCLE

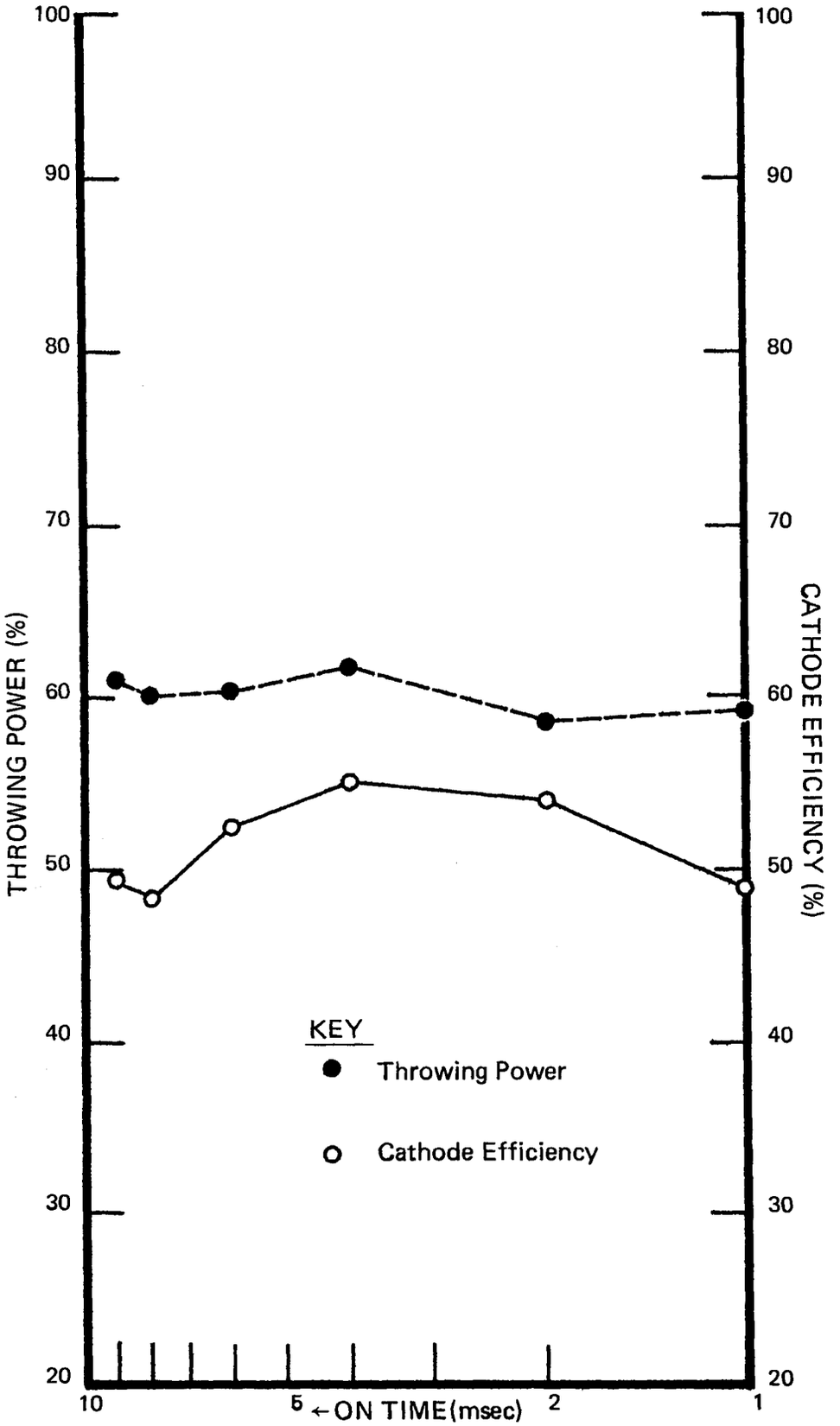

FIG. 52: THROWING POWER vs. LOG ON TIME AND CATHODE EFFICIENCY vs. LOG ON TIME FOR 66%, 75%, AND 90% DUTY CYCLES

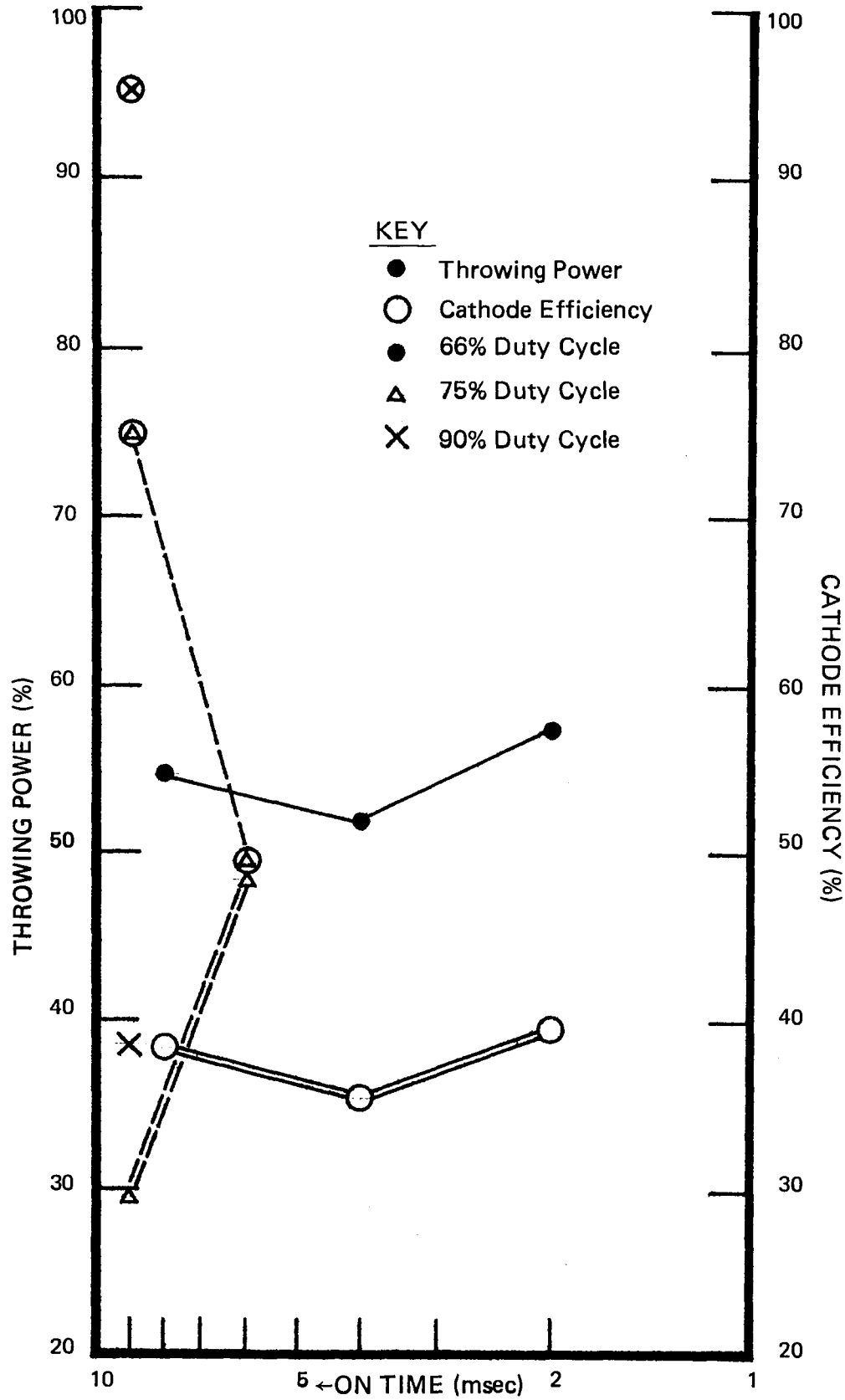

evolution occurs.

The overpotential for hydrogen evolution is reached at the long ON times. The concentration of depositing species, a gold complex, at the cathode interface is only a fraction of the species concentration in the bulk solution. As these species are depleted by deposition the resistance at the cathode increases. In other words, the limiting rate of mass transfer of the deposition species governs charge transfer. Greater voltage is required to maintain constant current flow and the potential for hydrogen evolution is reached as the depositing ions are depleted at long ON times. The increase in throwing power suggests the overpotential for H_2 evolution is being reached preferentially in the specimen areas which experience higher deposition rates at lower duty cycles not accompanied by H_2. There is an improvement in the distribution for deposition accompanying the hydrogen liberation. The improvement in throwing power is not of practical value, however, since the deposit is spongy and brown as a result of the H_2 evolution, making it unsuitable in most applications of gold deposits.

IX. Waveform

A. Introduction

The affect of the waveform on the characteristics of gold deposition system is the principle aim of this thesis. There are effects, however, of the plating system on the waveform. The purpose of this section is to characterize and to gain understanding of the waveform.

B. Electrochemical Circuit

A plating system has the properties of an electrical circuit. True square wave pulses, generated by a power supply, can be deformed by the circuitry of the solution. An equivalent system for consideration in conjunction with pulsed systems has been proposed by Haynes.[55] The circuit for each electrode is illustrated in Figure 53.

Polarization and an accompanying capacitance occurs at the electrode-electrolyte interface. Arrays of charged particles and molecules, i.e. ions and dipoles exist at the interface. This area is termed the electrical double layer; it is illustrated in Figure 42. The potential required to induce a reaction at irreversible electrodes is the activation polarization. Charging of the double layer capacitance is a contribution of the activation polarization. The polarization across the metal-electrolyte interface also results from changes in concentration at interface. The concentration polarization occurs due to the concentration gradient between the solution at the interface and that in the bulk electrolyte. Both concentration and activation polarization produce a capacitance at the interface denoted by, C, in Figure 53. The capacitance is frequency dependent since all RC circuits have a capacitative time constant; i.e. a finite time to charge.

A resistance, R, also exists in parallel to capacitance element of the equivalent circuit for the electrochemical system. A finite resistance exists at the interface due to processes of charge transfer. This resistance include ohmic polarization i.e. the IR drop at the

FIG. 53: ELECTROCHEMICAL CIRCUIT EQUIVALENT

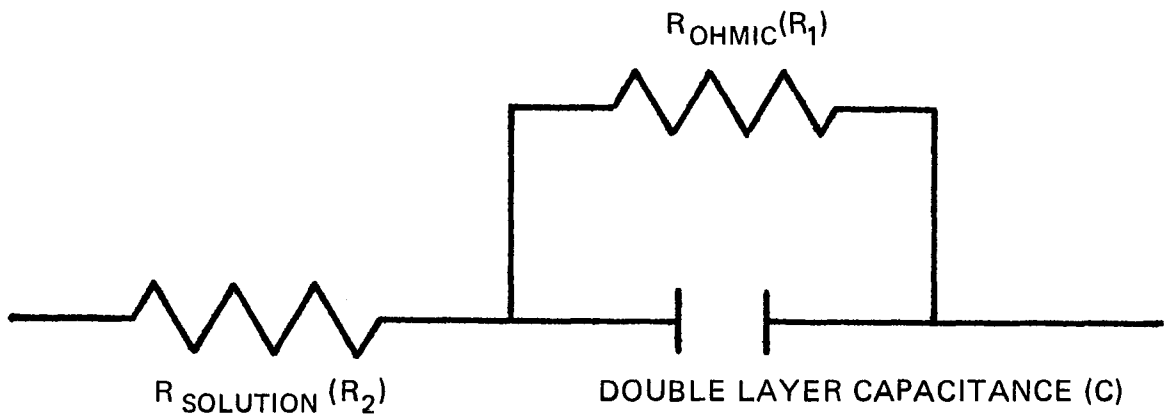

THE TOTAL CURRENT IS DEPENDENT ON THE FARADAIC AND THE CAPACITANCE COMPONENTS:

$$i = i_F + i_C$$

WHERE

$$i_C = C \frac{dV}{dt}$$

AND i_f IS DEPENDENT UPON THE CHEMISTRY AND REACTIONS OF THE SYSTEM.

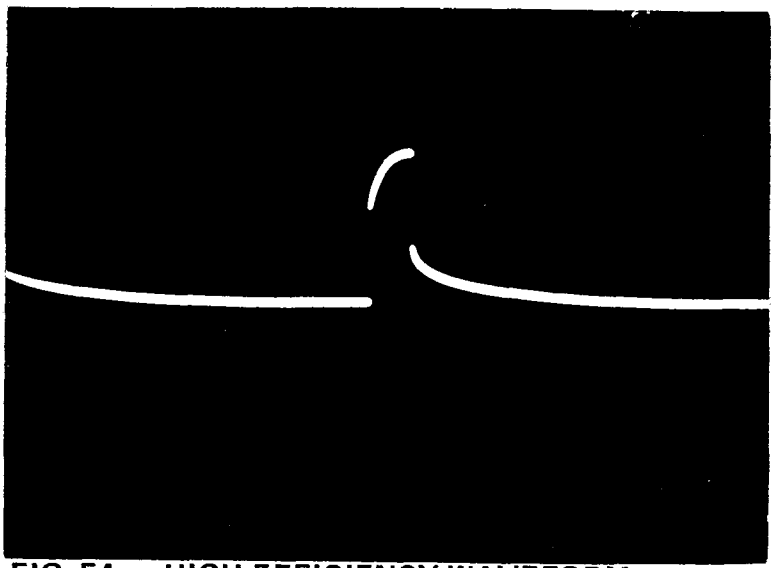

FIG. 54 HIGH EFFICIENCY WAVEFORM

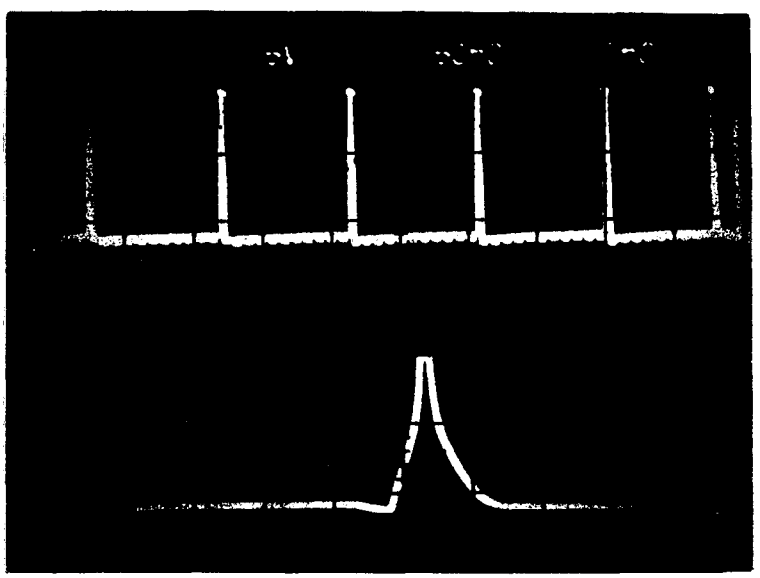

FIG. 55 LOW EFFICIENCY WAVEFORM

interface.

Another resistance, R_2, is in series with R_1 and C. This resistance is the ohmic drop of the bulk electrolyte. The mass transfer rate in this electrolyte, which has a different ion concentration than at the interface, primarily governs this resistance. Both R_1 and R_2 will be collectively referred to as the Faradadic resistance.

The total current, i_T, is the sum of the capacitance, i_C and the Faradadic component, i_F, at constant load:

$$i_T = i_C + i_F$$

where $i_C = C \frac{dv}{dt}$

$$i_F = \frac{R_1}{E_1} + \frac{R_2}{E_2}$$

C. Waveform at High Cathode Efficiencies

The distortion of the voltage waveform from true square is illustrated in Figure 54. The voltage, $\frac{dv}{dt}$, is characteristic of the capacitative affect on the square wave pulse. This oscillogram was recorded during deposition at 1 msec ON 9 msec OFF, which had a measured cathode efficiency of 100%. The high cathode efficiency suggests that metal deposition occurs during discharge of the capacitance. If this was not the case and other charge dissipation mechanisms operated, the cathode efficiency as a measure of deposition would be lowered.

D. Waveform Resulting in Low Cathode Efficiency

Specimens were deposited with a power supply having a sluggish potential rise time. The waveform which was recorded is shown in Figure 55. The waveform is more triangular than square. The fraction of current actually contributing to deposition is dependent upon the rapid rise in voltage in order to overcome polarization and drive adions through the

double layer to lattice sites. Although the power supply being considered was marketed as a pulse plating rectifier, cathode efficiencies of less than 25% were repeatedly obtained under the same conditions which produced 100% efficiency with rapid-rise rectifiers. The low efficiency indicates the potential required for metal deposition was not reached during a significant fraction of the pulse-ON time. Hydrogen evolution never occurred during the deposition indicating reactions requiring less energy, such as dipole rotation, deformed the voltage pulse.

X. Summary and Conclusions

Gold electrodeposits, particularly those used in electronic technology, are specified to meet exacting requirements. Pulse plating has recently become a viable industrial process as a result of the commercial availability of pulse power rectifiers with high amperage outputs. This process has promised new degrees of freedom to vary the properties of gold deposits. Characterization of gold films formed by pulse plating has lagged behind the availability of the commercial pulse rectifiers. The experimental work reported in these pages has aimed at characterizing selected properties which reflect the nature of pulse deposition at fixed plating conditions i.e. constant average current density and fixed bath parameters.

Porosity was decreased in the pulse plated deposits by comparison to gold deposits formed by evaporation, D. C. plating, and asymmetric A. C. plating. Examination of the microstructures of the films indicated pulse plated gold consisted of grains which were more densely packed and coalesced than films formed by the other deposition methods.

An examination of the effect of the pulse's characteristics on porosity was made for 30 waveforms. At low duty cycles, i.e. 9% and 33% the differences in thickness produced by the waveform were the predominant factor influencing porosity; the porosity increased as the thickness distribution became greater. At the 50% duty cycle porosity increased with increasing ON time but thickness distribution decreased with increasing ON time. At duty cycles greater than 50% neither correlations between porosity and thickness distribution nor ON time could be made. Efforts to diminish porosity are particularly applicable to reducing thickness requirements and therefore reducing the cost of gold protective layers.

The examination of thickness distribution dispelled the published conjectures that pulse plating produces a deposit with greater thickness uniformity than D. C. plated gold.

Less than 20% of the pulse deposits had greater uniformity than D. C. deposits. In the case of this 20% the increase in uniformity was marginal, well within experimental error.

Detailed study of the microstructure and crystallographic orientation of pulse plated gold by scanning electron microscopy and x-ray diffraction revealed patterns in these characteristics which were dependent on the pulse waveform. Models were suggested which correlate grain size and crystallographic orientation to nucleation conditions which are dependent on the nature of the electrical pulse. At long duty cycles i.e. >50%, where the crystallographic orientation was constant, the grain size increased with ON time. At short duty cycles i. e. 50%, where changes in crystallographic orientation occurred, the grain size was proportional to the duty cycle and inversely proportional to the ON time. This relation was deduced through the effect of (200) orientation on the nucleation rate for crystal growth. Knowledge of these fundamental structural differences which are dependent upon the pulse waveform, is a basis for understanding qualitative differences in the formation of pulse deposits.

Internal stress can be a source of failures in any application where adhesion is marginal. The stressed condition in pulsed deposition was studied and compared to D. C. deposition. While D. C. was constantly tensile with increasing thickness, pulse deposits became compressively stressed as thickness increased. The fine grain size and instantaneously high current densities were suggested as the factors necessary for a sorption mechanism of compressive stress to operate in pulse plated deposits.

The throwing efficiency or throwing power of pulse plating is greater than D. C. with certain pulse waveforms, less at other waveforms. The throwability was also linked to cathode efficiency; the two characteristics are parallel to one another. At long ON times, e.g. 8 and 9 msec ON, exceptions existed. In these cases cathode efficiency dropped, hydrogen evolution occurred, and a brown deposit formed; throwing

power, however, increased. Best throwing ability coupled with high cathode efficiencies and bright gold deposits was at short duty cycles i.e. 9% and 33%.

The rectifier used to produce the pulse has a pronounced effect on cathode efficiency. A rapid rise in voltage through the electrochemical system is necessary if the pulsed current is to be efficiently used for electrodeposition.

In conclusion, gold deposits formed by pulsed current have specific characteristics uncommon to other deposition methods. Pulses can be produced with a multitude of frequencies, durations, and magnitude. From the observations made by exploring 30 pulse conditions, porosity, thickness distribution, microstructure, crystallographic orientation, throwing efficiency, and cathode efficiency are all affected by the pulse waveform. The potential of pulse deposition is in its capability to alter deposit properties by simple electronic variation, rather than by involved chemical variations, the more traditional approach to controlling electrodeposition.

List of References

1. Langbein, G. and W. T. Brannt, Electrodeposition of Metals, 4th ed. Philadelphia: Henry Carey, Baird, p. 3, 1902.

2. de la Rive, A., Compt. Rend., 4, 835 (1837).

3. Wolhwill, British Patent 6,276 (1909).

4. Rosing, B., Z. Electrochem, 2, 550 (1896).

5. Gillis, J. H., U. S. Patent 1,260,661 (1917).

6. Madsen, C. P., U. S. Patent 1,583,891 (1910).

7. Pedersen, A. Z., U. S. Patent 1,574,055 (1920).

8. Huggins, N., U. S. Patent 1,527,734 (1922).

9. Holt, F. A., U. S. Patent 1,534,709 (1924).

10. Winkler, J., German Patent 576,585 (1931).

11. Girard, R., "Electrodeposition of Thin Magnetic Films", French Atomic Energy Commission, Grenoble Center of Nuclear Studies, June 10, 1965.

12. Leidheiser, H., Jr. and A. R. P. Ghuman, J. Electrochem, Soc., 120 (4), 484 (1973).

13. Baeyens, P., Trans. Inst. Met. Finishing, 31, 429 (1954).

14. Wan, C. C., H. Y. Cheh, and H. B. Linford, Plating, 559 (1974).

15. Cheh, H. Y., J. Electrochem. Soc., 118, 551 (1971).

16. Cheh, H, y., ibid, 1132 (1971).

17. Ozerov, A. M., N. P. Livitshko, I. N. Vavilina, P. M. Chetvertnov and Ya. E. Zhak, J. Appl. Chem, USSR, 40, 1101 (1967).

18. Avila, A. J. and M. J. Brown, Plating, 57, 1105 (1970).

19. Krivstov, A. K. and T. Ivanovek, Khim. Tekh. Inst., 7, 87 (1958).

20. Litvishko, N. P. and A. M. Ozerov, Chem. Abstr., 66, 9115 (1965).

21. Gnusin, N. P. and Ya. Kovarski, Electrokhim., 1, 46 (1965).

22. Popkov, A. P., Zh. Prikl. Khim., 39, 1747 (1966).

23. Gurovich, R. J. and A. K. Krivstov, Zh. Prikl. Khim. (Leningrad), 41 , 1227 (1969).

24. Lamb, V. A., Plating, 56 , 909 (1969).

25. Kroedler, A., Galvanotechnik, 61 (4), 290 (1970).

26. Krugliov, S. S., N. T. Kudryautsev, R. P. Sobolev and A. Ya. Antonov, Plating, 53, 78 (1966).

27. Walton, R. F., Plating, 53 (2), 209 (1966).

28. Krumbein, S. J., IEEE Trans. Parts Mater. Packaging, 5 (2), 89 (1969)

29. Krumbein, S. J., and M. Antler, IEEE Trans. Parts Mater. Packaging, 4 (1), 3 (1968).

30. Garte, S. M., Plating, 53 (11), 1335 (1966).

31. Garte, S. M., Plating, 55 (9), 946 (1968).

32. Leeds, J. M. and M. Clarke, Trans. Inst. Metal Finishing, 46 (1), 1 (1968).

33. Nobel, F. I., B. D. Ostrow, and D. W. Thompson, Plating, 52 (10), 1001 (1965).

34. Ashurst, K. G. and R. W. Neale, Trans. Inst. Metal Finishing, 45 (2), 75 (1967).

35. Leeds, J. M., Trans. Inst. Metal Finishing, 47 (5), 222 (1969).

36. Leeds, J. M. and M. Clarke, Trans. Inst. Metal Finishing, 43 , 50 (1965).

37. Ibid, 46 (1), 1 (1968).

38. Bockris, J. O'M., and A. Damjanovic, Modern Aspects of Electrochemistry, Vol. 3, London and Washington: Butterworths, p. 224, 1964.

39. Conway, B. E. and J. O'M. Bockris, Electrochem. Acta., 3, 340 (1960).

40. Vook, R. W. and F. Witt, J. Vac. Sci. Tech., 2 , 243 (1965).

41. Crandall, S. H. and W. C. Dahl, An Introduction to the Mechanics of Solids, New York: McGraw-Hill, p. 224, 1959.

42. McClintock, J. E. -- Private Communication, Western Electric Co., Princeton, N.J.

43. Cullity, B. D., Elements of X-Ray Diffraction , Ms.: Addison-Wesley, p. 72, 1956.

44. Walton, D., Phil. Mag., 7, 1671 (1962).

45. Brenner, A. and Senderhoff, J. Res. Nat. Bur. Standards, 42 , 82 (1949).

46. Van Der Merwe, J. H., Proc. Phys. Soc., A63 , 616 (1950).

47. Van Der Merwe, J. H., J. Appl. Phys., 31 , 117 (1963).

48. Matthews, J. W., Phil. Mag., 13, 1207 (1966).

49. Thompson, E. R., PhD. Dissertation, Univ. of Virginia, 1966.

50. Murbach, H. P. and H. Wilman, Proc. Phys. Soc. (London) B66 , 905 (1953).

51. Popereka, M. Ya., Phys., Met. Metallog., 20 , (5), 114 (1965).

52. Maki, K., Y. Nakajima, and K. Konosita, J. Vac. Sci. Tech., 6 (4), 622 (1969).

53. Law, S. S. and R. C. Sun, Thin Solid Films, 10 , 273 (1972).

54. Haynes, R. -- private communication, Western Electric Co., Princeton, N.J.

55. Haring, H. and W. Blum, Trans. Electrochem. Soc., 44 , 313 (1923).

56. Pan, L., Trans. Electrochem. Soc., Preprint, 58 (1930).

57. Iyer, S. Venkatakrishna, S. Hasmath Ibrahim, S. R. Rajagopalan and A. K. N. Reddy, Electroplating Metal Fin., 17, 159 (1964).

58. Subramanian, R., Electroplating Metal Fin., 5 (6), 29 (1969).

Appendix: Plating Procedure

I. Cleaning

Samples were plated on brass Hull cell panels, except where noted in the text. The panels were cleaned before deposition by the following procedure:

1. Removal of protective plastic coating
2. Acetone Rinse - 5 minutes
3. Methanol Rinse - 5 minutes
4. H_2O Rinse - 5 minutes
5. 15% HCl Dip - 2 minutes
6. H_2O Rinse - 5 minutes
7. Second H_2O Rinse - 5 minutes

II. Bath Chemistry

Deposition was carried out in an Ehrhardt type bath. The bath had the following chemical composition:

75 g/l dibasic ammonium citrate

75 g/l ammonium sulfate

20 g/l potassium gold cyanide

III. Bath Parameters

The pH was maintained at constant 5.0-5.5 with additions of citric acid or potassium hydroxide, whichever was appropriate. The agitation was vigorous and constant from an external pump and a magnetic stirrer. Temperature was maintained at 60 ° C and average current density at 5 amps/ft^2.

IV. Power Supply

The power supply was a Pulsco, Co. 2010 Pulse Unit. The low efficiency supply, described in the waveform section, was a Chem-O-Tronics, Chem-O-Plate 9.9 amp. pulse power supply. The leads from supply to electrodes were twisted and kept as short as feasible to minimize RC effects. A Tektronix oscilloscope was coupled to the electrodes

to continuously monitor the voltage waveform.

V. Final Cleaning

Following deposition all samples were cleaned with a cascade H_2O rinse, followed by two distilled H_2O dip rinses, then air dried.

Vita

David L. Rehrig was born in Allentown, Pennsylvania, April 8, 1947. He graduated from Lafayette College in 1969 with a Bachelor of Science Degree in Chemistry.

From 1969 to the present, he has been employed by Western Electric Co., Allentown as a development engineer in the device chemistry development laboratory. In June 1974 he was awarded the American Electroplater's Society Papers and Publication Committee Award for excellence in the presentation of a technical paper. He is a member of the American Chemical Society.